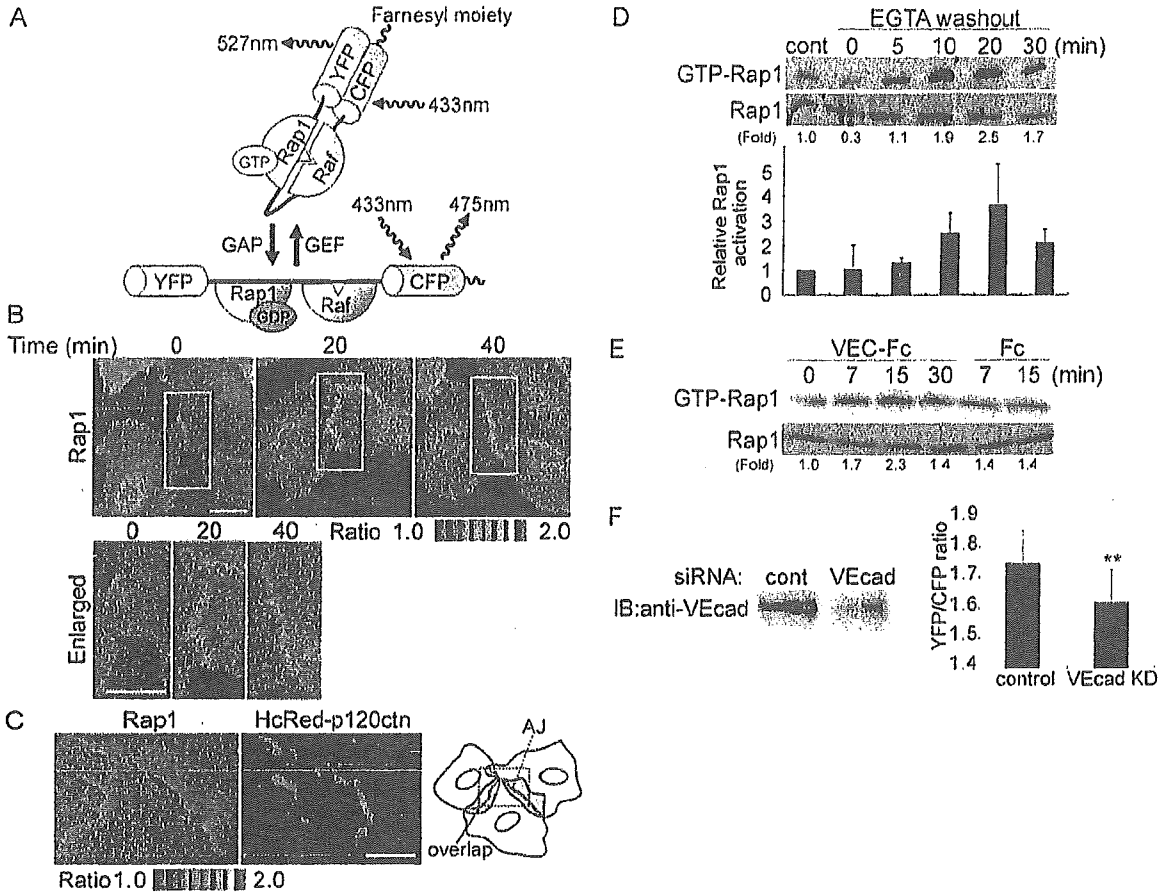

Figure 1. Rap1 is activated by VE-cadherin-mediated cell adhesion upon cell–cell contact. (A) Schematic illustration of Raichu-Rap1. FRET efficiency depends on the guanine nucleotide binding state of Rap1. GDP-bound Raichu-Rap1 emits 475-nm fluorescence when excited at 433 nm, whereas GTP-bound Raichu-Rap1 emits 527-nm fluorescence due to FRET. *Raf*; Ras/Rap1 binding domain of Raf. (B) Motile HUVECs infected with Adeno-Raichu-Rap1 were monitored by FRET time-lapse imaging every 20 s. A ratio image of YFP to CFP reflects FRET efficiency. Ratio images are shown by the intensity modulated display, in which the upper and lower limits of the ratio (the intensity of YFP divided by that of CFP) are indicated by the red and blue hues, respectively, and the average intensity of YFP and CFP is used. Time since starting FRET imaging is indicated on the top (min). The boxed regions in the top panels were enlarged and are shown in the bottom panels. Bars, 20 μm. (C) HUVECs expressing both Raichu-Rap1 and HcRed-tagged p120 catenin were FRET-imaged and red-fluorescence-imaged. The real images of boxed region of the schema are shown as FRET image (left panel) and red-fluorescence image (center). Areas indicated by the gray are regions where protruding and overlapping regions of the contacting cells. Note that Rap1 is activated at the adherens junctions where p120 catenin localizes. Bar, 20 μm. (D) Confluent HUVECs cultured in medium 199 containing 1% BSA without serum were treated with EGTA for 30 min to disrupt Ca^{2+}-dependent cell adhesion. Subsequently, the cells were treated with Ca^{2+}-containing medium. Cell lysates at the time points indicated at the top were subjected to pulldown assay for detecting GTP-bound Rap1 as described in *Materials and Methods*. A representative results from three independent experiments is shown (top). Fold activation indicates the ratio of the GTP-Rap1 intensity of total Rap1 intensity to the control GTP-Rap1 intensity of total Rap1 intensity. The result from three independent experiments were shown (bottom). Control (cont) was prepared from cells in medium 199 before calcium switch. Cells treated with EGTA for 30 min (time 0). (E) HUVECs sparsely cultured on the dish were stimulated with 10 μg/ml VEC-Fc or Fc for the time indicated at the top. Rap1 activity was examined as described for D. Fold activation is analyzed similarly to D. (F) The effect of VE-cadherin siRNA on VE-cadherin expression was examined by immunoblotting (left). FRET at the cell–cell contacts were quantitatively analyzed in control siRNA-treated HUVECs and VE-cadherin-depleted HUVECs (right), as explained in Supplementary Figure 2. Mean values with SDs obtained by 30 cell–cell contact sites are shown as a representative result of three independent experiments. Statistical significance was analyzed by Student's *t* test; ** $p < 0.01$.

with 10 μg VEC-Fc or Fc protein/ml in PBS-Ca^{2+}/Mg^{2+} overnight at 4°C followed by blocking with 1% heat-inactivated BSA in PBS (inactivated at 85°C for 12 min) for 1 h at room temperature. HUVECs treated with control siRNAs or MAGI-1 siRNAs were cultured for 48 h and then suspended in 0.5% BSA-containing Medium 199. Resuspended cells, 2.0×10^5, were plated and adhered onto each VEC-Fc- or Fc-coated well at 37°C for the indicated time. To analyze cell adhesion to a collagen-covered surface, a collagen-coated 24-well plate (Iwaki, Japan) was used instead of the VEC-Fc-coated plate. After washing with PBS-Ca^{2+}/Mg^{2+} four times to remove nonadherent cells, adherent cells and input cells were quantified by measuring endogenous alkaline phosphatase (ALP) activity by using AttoPhos AP fluorescent substrate system (Promega, Madison, WI).

RESULTS

Rap1 Is Activated on Homophilic VE-Cadherin Association at Cell–Cell Contacts

Rap1 is previously reported to localize to cell–cell contacts in vascular endothelial cells as well as epithelial cells to stabilize cell–cell contacts (Mandell *et al.*, 2005; Wittchen *et al.*, 2005). However, it remains elusive where Rap1 is activated on cell contacts. To monitor the spatiotemporal activation of Rap1 on vascular endothelial cell–cell contact,

HUVECs expressing Raichu-Rap1 were time-lapse FRET-imaged. Raichu-Rap1 consists of YFP, Rap1, the Ras-binding domain of Raf, CFP, and a CAAX box of Ki-Ras. The intramolecular binding of GTP-Rap1 to Raf induces FRET from CFP to YFP (Figure 1A), whereas the dissociation of Rap1 from Raf reduces FRET. Increased FRET indicated by a red hue was observed at cell–cell contacts during spontaneous movement (Figure 1B and Supplementary Movie 1). Rap1 was constantly activated in the perinuclear region of the cells irrespective of cell–cell contact.

In vascular endothelial cells, the peripheral membrane of cells contacting each other was overlapped. Thus, AJs and TJs are intermingled (Dejana, 2004). To ascertain Rap1 activation at the adherens junctions, HUVECs expressing both Raichu-Rap1 and HcRed-tagged p120 catenin were imaged (Figure 1C). Most of Rap1 activation as indicated by red hue was observed at AJs where p120 catenin was localized. No remarkable Rap1 activation was detected within the protruding membrane overlapping region.

We further quantitatively examined whether the Rap1 is activated during cell adhesion after de-adhesion by chelating extracellular calcium and restoring calcium (hereafter, calcium switch). GTP-bound Rap1 was rapidly increased within 5 min and to a greater extent than the predisruption level by restoration of Ca^{2+} (Figure 1D, top panel). The quantitative results obtained from three independent experiments were shown (Figure 1D, bottom panel). These results suggest that the cell–cell contact triggers the Rap1 activation in a manner dependent on extracellular Ca^{2+}. Although Rap1 is reported to be activated in a manner dependent on nectin, which is independent of extracellular Ca^{2+} (Fukuyama *et al.*, 2005), we assumed that Ca^{2+}-dependent cell–cell contact triggers Rap1 activation besides nectin-triggered Rap1 activation. We, therefore, examined the VE-cadherin engagement-dependent Rap1 activation. To mimic the VE-cadherin engagement in nascent cell–cell contacts, we used VEC-Fc chimeric protein, which consisted of the extracellular domain of VE-cadherin fused to the Fc portion of Ig. GTP-bound Rap1 was increased when cells were treated with VEC-Fc, but not with control Fc (Figure 1E).

To examine the requirement of VE-cadherin for Rap1 activation upon cell–cell contact, we imaged Rap1 activation in VE-cadherin-depleted HUVECs. Quantitative FRET imaging analysis upon cell–cell contacts demonstrated that Rap1 activation at the cell–cell contacts was less in VE-cadherin-depleted cells than those observed in control siRNA-treated cells (Figure 1F). Collectively, these data indicate that the engagement of VE-cadherin induces Rap1 activation.

MAGI-1 Localizes to Cell–Cell Contacts and Binds to β-Catenin

MAGI-1 constitutes a complex with E-cadherin/β-catenin and associates with a GEF for Rap1, PDZ-GEF1 (Kawajiri *et al.*, 2000), implying that MAGI-1 may link the cadherin-mediated signal to PDZ-GEF1 for the activation of Rap1. To investigate the involvement of MAGI-1 in Rap1 activation on VE-cadherin-mediated cell–cell contact, we first developed an anti-MAGI-1 antibody and examined the expression of MAGI-1 in vascular endothelial cells. MAGI-1 was expressed in all cultured vascular endothelial cells we tested, because it was found in MDCK epithelial cells used as a positive control (Figure 2A). Next, we examined the localization of MAGI-1 in vascular endothelial cells by immunostaining. MAGI-1 was localized to the cell–cell contacts (Figure 2B) and colocalized with VE-cadherin (Figure 2C). The immunopositive reaction in the nucleus appeared to be non-

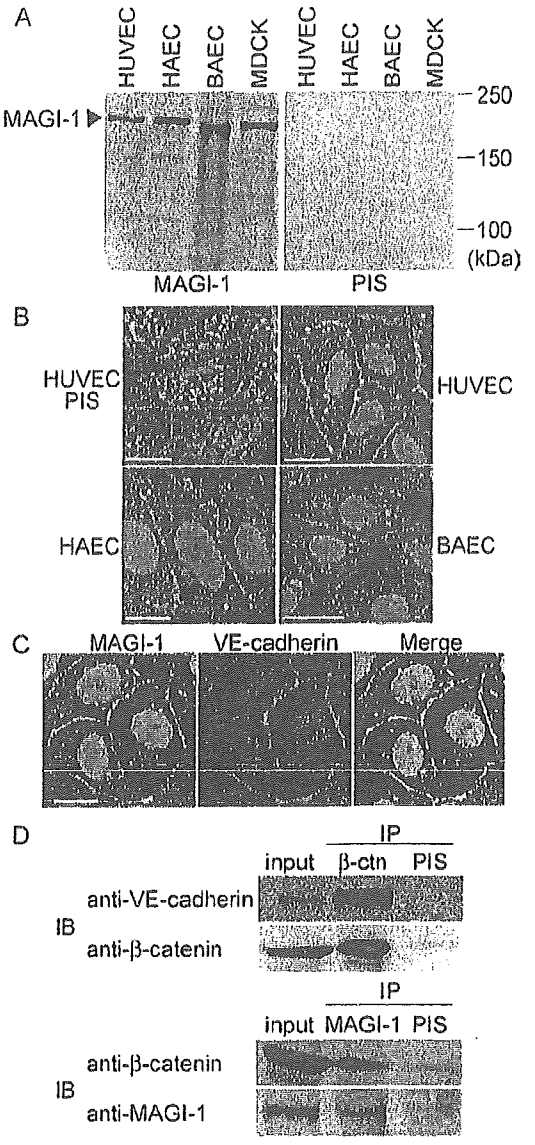

Figure 2. MAGI-1 localizes to cell–cell contacts and forms a complex with VE-cadherin and β-catenin. (A) Lysates from the cells indicated at the top were subjected to SDS-PAGE followed by immunoblotting with anti-MAGI-1 antibody (left) and with pre-immune serum (PIS, right). (B) Endothelial cells were immunostained with pre-immune serum (PIS, left top) and anti-MAGI-1 antibody. Immunoreaction was visualized by fluorescent microscopy. Bars, 20 μm. (C) HUVECs were immunostained with both anti-MAGI-1 antibody (green) and anti-VE-cadherin antibody (red). A merged image is shown in the right panel (Merge). Bar, 20 μm. (D) Cell lysates from HUVECs were subjected to either immunoprecipitation (IP) with antibodies as indicated at the top followed by immunoblotting (IB) with antibodies as indicated at the left. VE-cadherin was coimmunoprecipitated with β-catenin (top). β-catenin was coimmunoprecipitated with MAGI-1 (bottom)

specific, because it was detected in the nucleus by immunostaining using preabsorbed anti-MAGI-1 (unpublished data) and after knockdown of MAGI-1 (see Figure 5B).

To investigate how MAGI-1 localizes to cell–cell contacts, we tested the link between VE-cadherin and MAGI-1 by β-catenin. We examined this link by immunoprecipitation

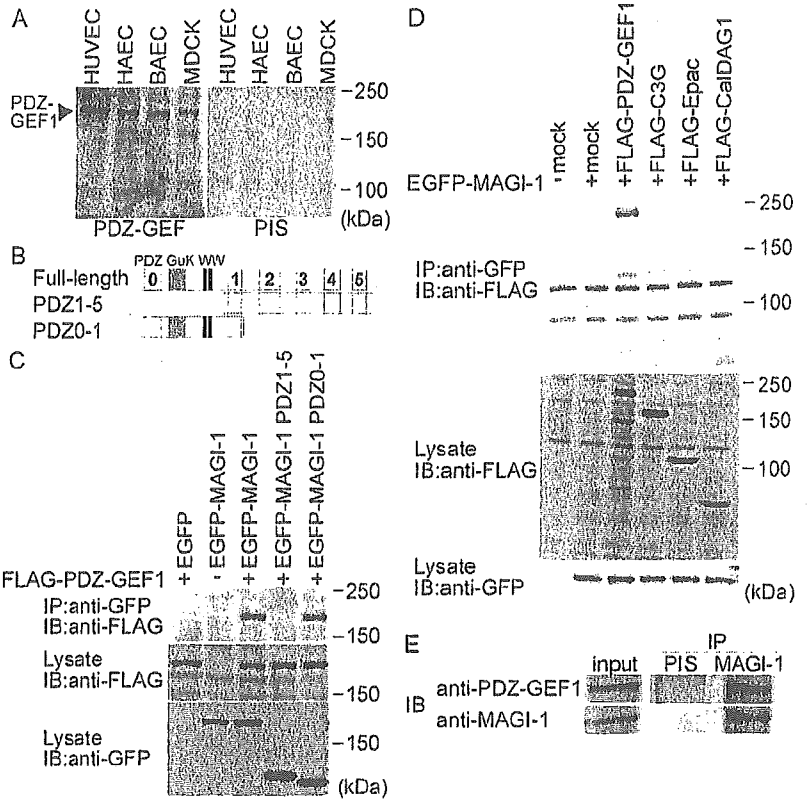

Figure 3. MAGI-1 interacts with PDZ-GEF1 in vascular endothelial cells. (A) Cell lysates from HUVECs, HAECs, BAECs, and MDCK cells were subjected to SDS-PAGE and immunoblotting with anti-PDZ-GEF1 antibody (left) or pre-immune serum (PIS, right). (B) Schematic illustration of MAGI-1 (full length) and its deletion mutants. MAGI-1 consists of six PDZ domains (PDZ0–5, indicated by gray boxes), a guanylate kinase domain (GuK), and two WW domains. Deletion mutants, PDZ1–5 and PDZ0–1, consist of PDZ1 to PDZ5 and the amino-terminus to PDZ1, respectively. (C) 293T cells were transfected with the plasmids together with (+) or without (−) FLAG-tagged PDZ-GEF1 expressing vector as indicated at the top. Cell lysates were subjected to immunoprecipitation (IP) with anti-GFP antibody followed by immunoblotting (IB) or directly to immunoblotting using the antibodies as indicated. Note that FLAG-tagged PDZ-GEF1 is coimmunoprecipitated with GFP-tagged PDZ0–1. (D) Cells transfected with a panel of FALG-tagged Rap1 GEF-expressing plasmids together with (+) or without (−) EGFP-tagged MAGI-1-expressing plasmid. Cell lysates were subjected to immunoprecipitation (IP) followed by immunoblotting (IB) similarly to C. Note that only FLAG-tagged PDZ-GEF-1 among several Rap1 GEFs is coimmunoprecipitated with MAGI-1. (E) The lysate of HUVECs was incubated with either pre-immune serum (PIS) or anti-MAGI-1 antibody, followed by immunoblotting with anti-PDZ-GEF1 antibody. Note that MAGI-1 is coimmunoprecipitated with PDZ-GEF1.

assay (Figure 2D). β-catenin bound to both VE-cadherin (Figure 2D, top panel) and MAGI-1 (Figure 2D, bottom panel). These results indicate that MAGI-1 appears to localize to VE-cadherin-based cell adhesion through β-catenin in vascular endothelial cells.

MAGI-1 Interacts with PDZ-GEF1 in Vascular Endothelial Cells

It has been shown that MAGI-1 binds to PDZ-GEF1 localized to cell–cell contacts in epithelial cells (Dobrosotskaya and James, 2000; Kawajiri *et al.*, 2000). We hypothesized that PDZ-GEF1 is associated with MAGI-1 in vascular endothelial cells and that it is involved in the activation of Rap1 on VE-cadherin-mediated cell–cell contact. PDZ-GEF1 was expressed in vascular endothelial cells similarly to MAGI-1 (Figure 3A). The interaction between MAGI-1 and PDZ-GEF1 was examined by the immunoprecipitation using the full-length and the truncated mutants of MAGI-1 (Figure 3, B and C). The PDZ-GEF1 bound to the N-terminus of MAGI-1 (Figure 3C). EGFP-tagged MAGI-1 coimmunoprecipitated PDZ-GEF1, but not other GEFs for Rap1, C3G, Epac1, and CalDAG-GEF-I (Figure 3D). We further examined the interaction between endogenous MAGI-1 and PDZ-GEF1 in HUVECs. Both MAGI-1 and PDZ-GEF1 were coimmunoprecipitated from the lysate of HUVECs (Figure 3E), indicating that PDZ-GEF1 associates with MAGI-1 in vascular endothelial cells.

Localization of MAGI-1 to Cell–Cell Contact is Important for Rap1 Activation on Cell Contact

To understand the role of MAGI-1 in activating Rap1 when forming cell–cell contacts, we proceeded to investigate the localization of MAGI-1 using EGFP-tagged MAGI-1 in motile endothelial cells. EGFP-MAGI-1 was accumulated at cell–cell contacts (Figure 4B, left panels, and Supplementary Movie 2). Removal of the carboxy terminal PDZ domain (delta PDZ5) resulted in the dissociation of MAGI-1 from cell–cell contacts (Figure 4B, right panels, and Supplementary Movie 3). Because it was reported that MAGI-1 binds to β-catenin through PDZ5 (Dobrosotskaya and James, 2000), we tested the requirement of PDZ5 for the association of MAGI1- with β-catenin. β-catenin was coimmunoprecipitated with EGFP-tagged full-length MAGI-1 but not with MAGI-1 lacking PDZ5 (Figure 4C). These results suggest that MAGI-1 localizes to vascular endothelial cell–cell contacts in a manner dependent on β-catenin. We further revealed that MAGI-1 was dislocated from the cell–cell contact of the PDZ5-expressing cells as marked by red fluorescence but not from that of wild-type cells (Figure 4D), indicating that PDZ5 is important for the localization of MAGI-1 to cell–cell contacts.

To examine the requirement of the association of MAGI-1 with β-catenin for the cell–cell contact-induced Rap1 activation, we checked the effect of disconnection of MAGI-1 to β-catenin by overexpressing MAGI-1 PDZ domain 5 on Rap1 activation. In HUVECs expressing MAGI-1 PDZ domain 5, as marked by dsFP593 (Figure 4E and Supplementary Movie 4), Rap1 activation upon cell–cell contacts was not observed in FRET imaging. These results indicate that the dislocation of MAGI-1 from the cell–cell contact inhibits Rap1 activation at the cell–cell contacts in motile vascular endothelial cells.

To confirm the requirement of MAGI-1 in Rap1 activation upon vascular endothelial cell–cell contact, we knocked down MAGI-1 in HUVECs using RNA interference. MAGI-1

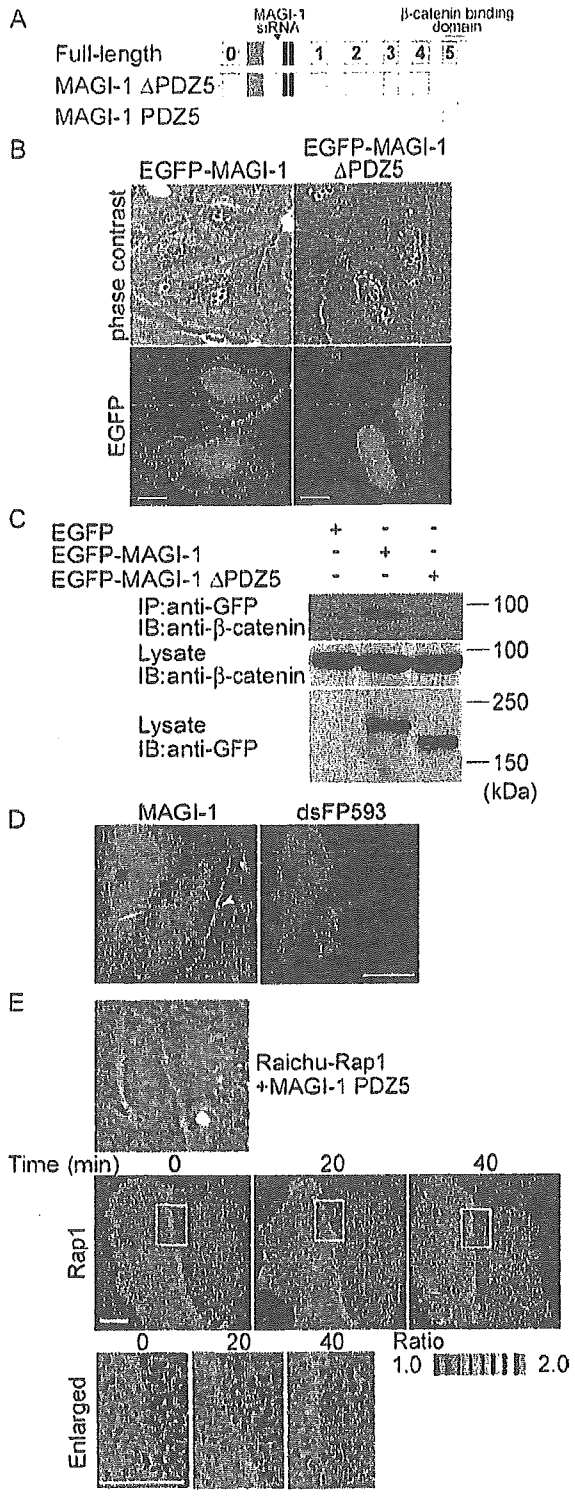

Figure 4. MAGI-1 localizing to cell–cell contact via β-catenin is required for Rap1 activation. (A) Schematic illustration of MAGI-1 and its mutants. The corresponding region of siRNA for MAGI-1 used in Figure 5 is also indicated in this schema.(B) HUVECs were transfected with the plasmids indicated at the top and imaged on an Olympus IX-81 fluorescent microscope. Bars, 20 μm. Note the localization of EGFP-MAGI-1 at the cell–cell contact but not MAGI-1 lacking PDZ domain 5. (C) 293T cells were transfected with the plasmids as indicated at the top. Cell lysates were subjected to immunoprecipitation (IP) with anti-GFP followed by immunoblotting (IB) or directly to immunoblotting using the antibodies indicated at the left. Note that endogenous β-catenin is coimmunoprecipitated with EGFP-tagged MAGI-1, but not with that lacking PDZ5. (D) HUVECs expressing PDZ domain 5 of MAGI-1 was immunostained with anti-MAGI-1 antibody. No immunoreaction was detected at the cell–cell contact between PDZ domain 5-expressing cells (arrow), whereas immunoreaction was detected at the contact between PDZ domain 5-expressing cell and untransfected cell (arrow-head). (E) HUVECs transfected with Raichu-Rap1 and pIRM21-MAGI-1–PDZ5 were FRET-imaged (middle). Phase contrast image was overlaid onto the image for dsFP593 to distinguish HUVECs transfected with pIRM21-MAGI-1–PDZ5 from those transfected only with Raichu-Rap1 (top). Red and blue hues indicated by intensity modulated display reflect increased and decreased FRET, respectively. The boxed regions in the middle panels were enlarged (bottom). The upper and lower limits of the ratio range are shown at the bottom right. Bars, 20 μm.

was almost completely reduced, as examined by Western blotting (Figure 5A). MAGI-1 at the cell–cell junction was not found in the cells treated with siRNA, as examined by immunostaining (Figure 5B). In the same setting, siRNA-introduced HUVECs expressing Raichu-Rap1 were subjected to FRET imaging. Rap1 activation upon cell–cell contact was significantly suppressed in MAGI-1-depleted cells (Figure 5C and Supplementary Movie 5). Quantitative FRET imaging analysis was performed to quantitatively analyze the activation of Rap1 at the cell–cell contacts in MAGI-1-depleted cells (Figure 5D and Supplementary Figure 2). We notice that Rap1 activation was detected at the free ruffled membrane without cell–cell contacts, similarly to control cells (Supplementary Movies 1 and 5), even in the MAGI-1-depleted cells. Collectively, these data suggest that the localization of MAGI-1 to cell–cell contacts through binding to β-catenin is involved in Rap1 activation.

Depletion of MAGI-1 Results in Impairment of VE-Cadherin-based Cell Adhesion

To elucidate the role of activated Rap1 downstream of MAGI-1 upon cell–cell contact, we examined the effect of depletion of MAGI-1 on VE-cadherin/β-catenin-based cell–cell contact after calcium switch. The localization of VE-cadherin and β-catenin at cell–cell contacts in confluent monolayer-cultured HUVECs was unchanged by MAGI-1 siRNA treatment. Because calcium switch induces cadherin-mediated cell junction after its disruption, we looked at the localization of VE-cadherin and β-catenin during calcium switch by immunostaining for VE-cadherin and β-catenin. VE-cadherin was reaccumulated at cell–cell junctions together with β-catenin within 20 min in control HUVECs. In clear contrast, there was a significant impairment of the formation of VE-cadherin/β-catenin-based cell junction in MAGI-1-depleted HUVECs (Figure 6).

TJ formation was not affected by MAGI-1 depletion and calcium switch (Figure 7A), whereas the recovery of VE-cadherin-based cell adhesion was substantially impaired in MAGI-1-depleted cells. These results indicate that MAGI-1-mediated signal is important for VE-cadherin/β-catenin-based cell adhesion.

We and others have previously reported that Rap1 activation enhances cell adhesions (Fukuhara *et al.*, 2005; Kooistra *et al.*, 2005). Cortical actin formation is enhanced by Rap1 activation and strengthens VE-cadherin-based cell–cell adhesion. Vinculin supports the cortical actin by linking α-catenin to α-actinin and by directly functioning as an

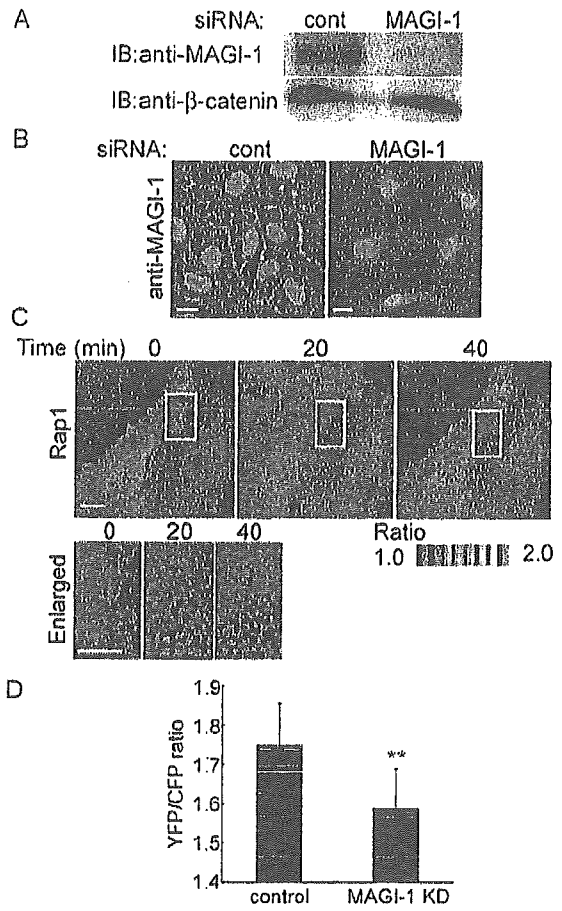

Figure 5. Depletion of MAGI-1 inhibits Rap1 activation upon cell–cell contact. (A) HUVECs transfected with control siRNAs or MAGI-1 siRNAs were cultured for 48 h. The cells were lysed, subjected to SDS-PAGE, and immunoblotted with anti-MAGI-1 and anti-β-catenin. (B) HUVECs transfected with control siRNAs or MAGI-1 siRNAs were cultured for 48 h and immunostained with anti-MAGI-1. Bars, 20 μm. (C) MAGI-1-depleted HUVECs were infected with Adeno-Raichu-Rap1 and FRET-imaged. The ratio-images indicate Rap1 activation by red hue and Rap1 inactivation by blue hue (top). The boxed region between two neighboring cells is enlarged (bottom). Bars, 20 μm. (D) Quantitative FRET analysis at the cell–cell contacts were performed in cells treated with control siRNA-treated HUVECs (control) and with MAGI-1-depleted cells (MAGI-1 KD). Quantitative FRET analysis is explained in Supplementary Figure 2. Mean values with standard deviations obtained by 30 cell–cell contact sites are shown as a representative result of three independent experiments. Statistical significance was analyzed by Student's *t* test and is indicated as $^{**}p < 0.01$.

actin-bundling molecule (Kobielak and Fuchs, 2004). Thus we investigated the vinculin localization after calcium switch by immunostaining. Vinculin was observed at the cell-ECM contacts presumably by translocating from cell–cell contacts after calcium depletion. Calcium restoration induced the relocation of vinculin from cell-ECM to cell–cell contact in control siRNA-treated cells. In clear contrast, vinculin remained at the focal adhesions in MAGI-1-depleted cells after calcium switch (Figure 7B). These data suggest that MAGI-1-dependent Rap1 activation at cell–cell contact may affect the vinculin localization, thereby regulating VE-cadherin-based cell adhesion.

MAGI-1 Is Required for VE-Cadherin-mediated Cell Adhesion

Vascular endothelial cell adhesion entails VE-cadherin-based adhesion and other cell adhesion molecules-based cell adhesion. To directly assess the involvement of MAGI-1 in VE-cadherin-mediated cell adhesion, we examined the adhesion of control siRNA-treated HUVECs and MAGI-1-depleted HUVECs onto VEC-Fc-coated dishes. The adhesion was quantified by the ALP activity of cells attaching to the dish after washing. Control HUVECs adhered to the VEC-Fc-coated dish in a time-dependent manner, whereas MAGI-1-depleted HUVECs exhibited significantly impaired adhesion to the VEC-Fc-coated dish (Figure 7A). No cells attached to the Fc-coated dish. MAGI-1-depleted HUVECs adhered to the collagen-coated dish comparably to control HUVECs (Figure 7B). We proceeded to examine the effect of inactivation of Rap1 on VE-cadherin-dependent adhesion. Control adenovirus-infected HUVECs adhered to VEC-Fc-coated dish, whereas Rap1GAPII-expressing adenovirus-infected HUVECs did not (Figure 7C). These results indicate that MAGI-1 and Rap1 activation is required for VE-cadherin-dependent cell adhesion.

DISCUSSION

FRET imaging enabled us for the first time to show the activation of Rap1 at the endothelial cell–cell junction, although previously Rap1 was suggested to be activated upon cell adhesion. In epithelial cells, C3G associating with E-cadherin is responsible for Rap1 activation upon cell contacts (Hogan *et al.*, 2004). Rap1, vice versa, regulates E-cadherin-mediated cell adhesion (Price *et al.*, 2004). In addition to E-cadherin, homophilic dimerization of nectin at the AJs triggers Rap1 activation downstream of Src-Crk (Fukuyama *et al.*, 2005). During the calcium switch experiment, which requires extracellular Ca^{2+}, we found that Rap1 was activated (Figure 1C), indicating extracellular Ca^{2+}-dependent signal, namely cadherin- and nectin-independent signal, appears to be involved in Rap1 activation upon cell–cell contact. In the present study, we propose the involvement of the MAGI-1/PDZ-GEF1 complex in Rap1 activation, besides nectin-mediated Rap1 activating signal and the subsequent positive feedback regulation of VE-cadherin-mediated cell adhesion.

Rap1 is responsible for maintenance and maturation of AJs. The establishment of cadherin-dependent cell–cell contacts is attributable to Rap1 in *Drosophila melanogaster* and mammalian cells (Knox and Brown, 2002; Price *et al.*, 2004). Consistently, we show here that VE-cadherin-dependent cell adhesion triggers a signal implicating MAGI-1 in Rap1 activation, presumably the MAGI-1–PDZ-GEF1-Rap1 pathway. VE-cadherin engagement-induced Rap1 activation may contribute to AJ formation in addition to homophilic engagement of nectin-dependent Rap1 activation (Fukuyama *et al.*, 2005).

Here we demonstrate VE-cadherin-dependent Rap1 activation besides nectin-dependent Rap1 activation. Calcium switch does not alter localization of nectin at the cell–cell contacts (Yamada *et al.*, 2005). We found that Rap1 was activated after calcium restoration in the calcium switch experiment that mimics nascent cell–cell contact formation (Figure 1), indicating that Ca^{2+}-dependent cell–cell contact is involved in Rap1 activation. We first assumed that VE-cadherin is responsible for Rap1 activation. Indeed, VE-cadherin depletion inhibited cell–cell contact-mediated Rap1 activation (Figure 1F).

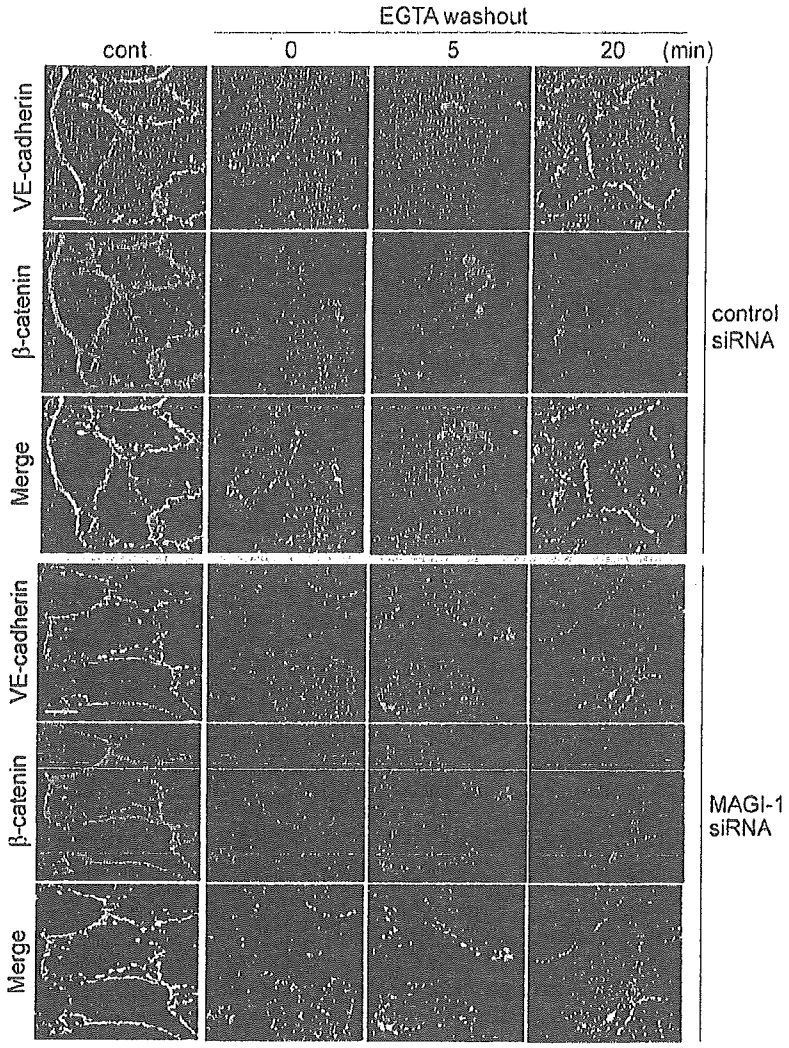

Figure 6. Depletion of MAGI-1 impairs AJ formation. HUVECs transfected with control siRNAs (top three columns) or MAGI-1 siRNAs (bottom three columns) were cultured for 48 h. Cells were replated onto the glass-base dishes for another 24 h to constitute the cell–cell contacts. The cells were treated with EGTA for 30 min to disrupt VE-cadherin-dependent junctions and kept in the replaced medium containing Ca^{2+} for the time indicated at the top. The cells were immunostained with anti-VE-cadherin antibody (green) and anti-β-catenin antibody (red). The merged images are shown in the bottom panels (Merge). Bars, 20 μm. VE-cadherin remarkably accumulated 20 min after Ca^{2+} restoration in control siRNA-treated HUVECs, whereas slight accumulation was observed in MAGI-1 siRNA-treated HUVECs.

These two AJ molecules, VE-cadherin and nectin, are linked by their cytoplasmic domain-associating proteins (Tachibana *et al.*, 2000). L-afadin, a nectin cytoplasmic domain-binding molecule, binds to α-catenin and subsequently locates cadherin to AJs without the transinteraction of cadherin (Tanaka *et al.*, 2003). L-afadin, s-afadin (AF-6), and Canoe (*Drosophila* orthologue of AF-6) contain a Rap1-binding domain (Boettner *et al.*, 2000, 2003). Thus, afadin regulated by activated Rap1 at cell–cell contacts may enhance AJ formation constituted by both cadherin and nectin.

We explored the requirement of MAGI-1 for Rap1 activation at cell adhesion. The association of MAGI-1 with β-catenin via the PDZ domain 5 is critical for its localization to VE-cadherin-based cell–cell contact. MAGI-1 also interacts with endothelial cell-selective adhesion molecule (ESAM) and JAM-4 at TJs (Hirabayashi *et al.*, 2003). Other JAM family members (JAM-A, B, and C) do not bind to MAGI-1 (our unpublished data). The carboxy-terminal sequence of ESAM and JAM-4 provides the class I PDZ-binding motif, whereas that of JAM family members contains the class II PDZ-binding motif (Hung and Sheng, 2002). Thus, ESAM-mediated MAGI-1 recruitment may contribute to Rap1-regulated cell adhesion at TJs as β-catenin recruits MAGI-1 at AJs. It will be interesting to explore the TJ-dependent Rap1 activation.

MAGI-1 together with MAGI-2 (S-SCAM), and MAGI-3 constitute the MAGI family (Hirao *et al.*, 2000; Franklin *et al.*, 2005). It has been shown that MAGI-2 binds to β-catenin and that MAGI-3 colocalized to β-catenin in astrocytes expressing E-cadherin (Adamsky *et al.*, 2003; Subauste *et al.*, 2005). Although MAGI-2 is exclusively expressed in the brain, MAGI-3 is ubiquitously expressed. Although we cannot exclude the involvement of MAGI-3 in the activation of Rap1 in vascular endothelial cells, the disconnection of MAGI family members from β-catenin by overexpressing the PDZ domain 5 of MAGI-1 perturbed the Rap1 activation upon cell–cell contact (Figure 4, D and E). Furthermore, depletion of MAGI-1 by siRNA hampered the Rap1 activation (Figure 5), suggesting that MAGI-1 is indispensable for Rap1 activation based on the linkage between VE-cadherin-β-catenin complex and MAGI-PDZ-GEF1 complex in vascular endothelial cells.

To delineate the VE-cadherin engagement-triggered Rap1 activation signal, we tried to test the requirement of

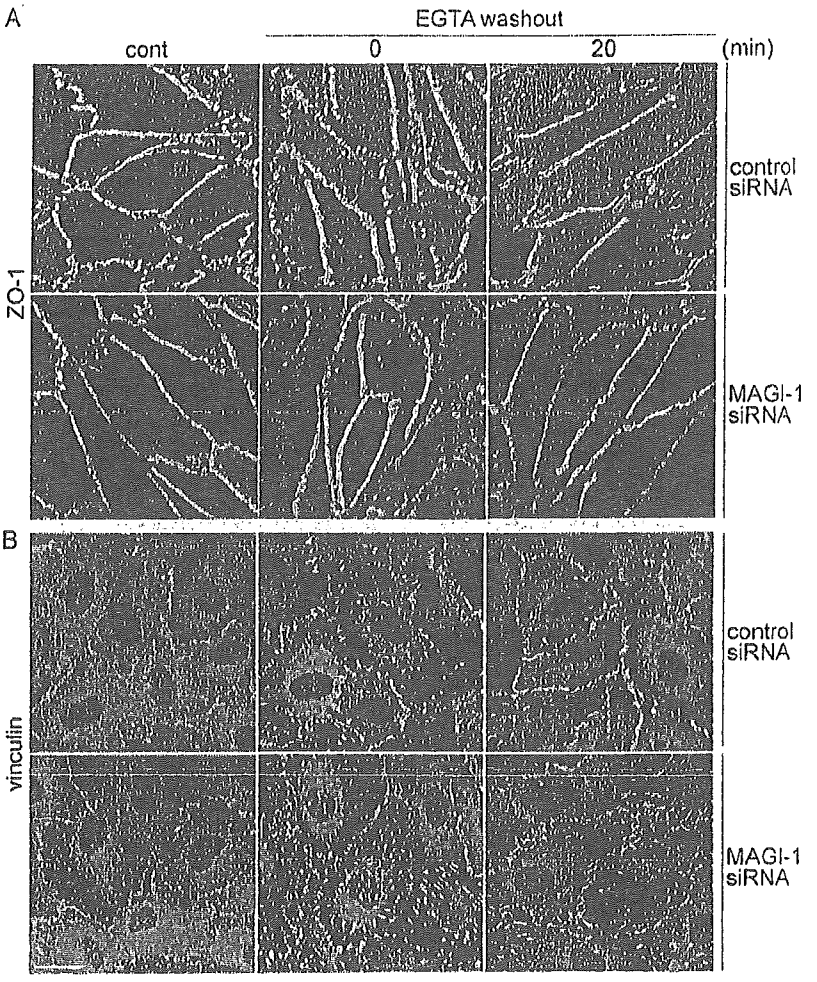

Figure 7. MAGI-1 depletion affects an AJ-supporting molecule, vinculin, but not a TJ-supporting molecule, ZO-1. (A) Similarly to Figure 6, HUVECs treated with control siRNAs (top panels) and MAGI-1 siRNAs (bottom panels) were immunostained with anti-ZO-1 after calcium switch. Bar, 20 μm. Note that ZO-1-positive cells were affected neither by calcium switch nor MAGI-1 depletion. (B) Similarly to A, control siRNA-treated cells and MAGI-1-depleted cells were immunostained with anti-vinculin before and after Ca^{2+} switch. Ca^{2+} depletion from the culture medium resulted in displacement of vinculin from cell–cell contacts to cell-ECM contacts and Ca^{2+}-restoration induced relocalization from cell-ECM contacts to cell–cell contacts in control HUVECs. In clear contrast, vinculin remained at the cell-ECM contacts even 20 min after Ca^{2+} restoration in MAGI-1-depleted cells.

PDZ-GEF1 for Rap1 activation because we found that MAGI-1 associated with PDZ-GEF1 in vascular endothelial cells (Figure 3), as this association reported previously (Dobrosotskaya and James, 2000; Kawajiri *et al.*, 2000). PDZ-GEF1-depleted cells seemed to be detached from the collagen-coated dishes and the adhesive activity to collagen-coated dish was significantly inhibited. Thus we assumed that there might be other signaling besides MAGI-1–PDZ-GEF1-mediated signal for cell adhesion and thus concluded that PDZ-GEF1-depleted cells were not appropriate for further evaluation to delineate the signaling. At least, VE-cadherin engagement-triggered Rap1 activation requires MAGI-1.

Activated Rap1 upon cell–cell contact further strengthens the VE-cadherin-dependent cell–cell adhesion. Rap1 activation is required for VE-cadherin-mediated cell adhesion (Figure 8B). We previously reported that the inside-out signal regulated by cAMP-Epac-Rap1 signal enhances the VE-cadherin-mediated cell–cell contacts by regulating cortical actin (Fukuhara *et al.*, 2005). Although we did not observe significant cortical actin distribution after calcium switch experiment (unpublished data), we noticed that the relocation of vinculin from cell-ECM to cell–cell contacts was inhibited in MAGI-1-depleted cells. Because vinculin supports the cadherin-based cell contacts by linking actin to cytoplasmic domain of cadherin through α-catenin, inhibition of Rap1 activation by MAGI-1 depletion might affect AJ formation. These results imply a positive feedback loop in cell–cell contact regulated by Rap1; namely, cell–cell contact promotes transdimerization of cell surface adhesion molecules, inducing Rap1 activation followed by further tightening of VE-cadherin-mediated cell adhesion.

In conclusion, we revealed that MAGI-1 is required for Rap1 activation upon cell–cell contacts and in turn for AJ formation. The translocation of MAGI-1 to cell–cell contacts is ascribed to its association with β-catenin. The MAGI-1-associating molecule, PDZ-GEF1, may account for Rap1 activation.

ACKNOWLEDGMENTS

We are grateful to M. Matsuda for his advice, plasmids, and virus; K. Kaibuchi for anti-PDZ-GEF1 antibody; J. T. Pearson for his critical reading of this manuscript; and M. Sone, Y. Mizushima, and Y. Matsuura for their technical assistance. This work was supported by grants from the Ministry of Health, Labor, and Welfare Foundation of Japan; from the Program for Promotion of Fundamental Studies in Health Sciences of the National Institute of Biomedical Innovation; from the Ministry of Education, Science, Sports and Culture of Japan; from the Mochida Memorial Foundation for Medical and Pharmaceutical Research; and from Astellas Foundation for Research on Metabolic Disorders.

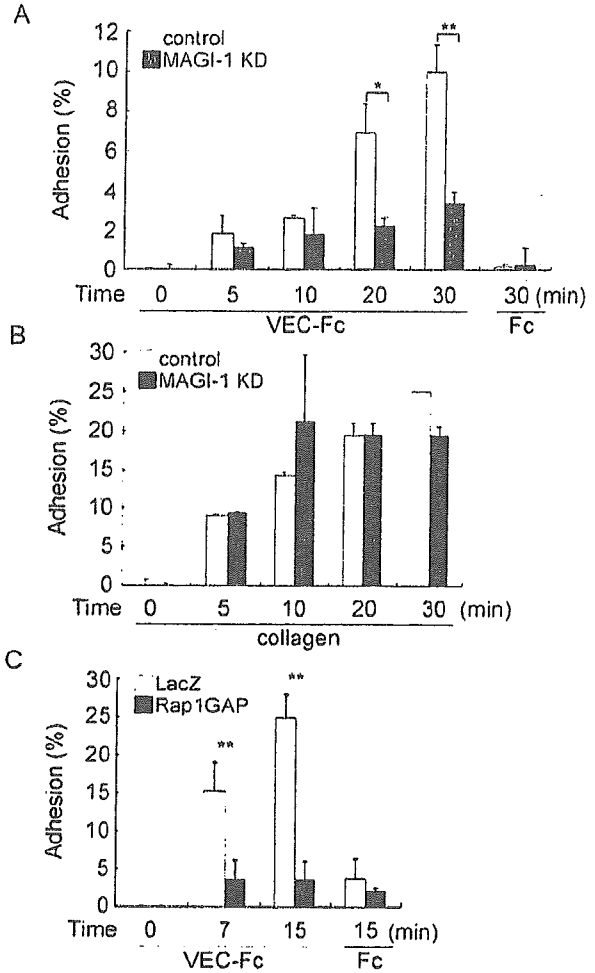

Figure 8. Depletion of MAGI-1 and inactivation of Rap1 inhibits VE-cadherin-mediated cell adhesion. (A) HUVECs transfected with control siRNAs (white column) or MAGI-1 siRNAs (black column) were cultured for 48 h, suspended in 0.5% BSA-containing medium 199, and incubated for 30 min at 37°C. Cells, 2.0×10^5, were plated onto either a VEC-Fc- or Fc-coated well for the time indicated at the bottom. Cell adhesion was quantified as described in *Materials and Methods*. The averages of triplicate (plus SDs) are presented. A representative result of three independent experiments is shown. Statistical significance was analyzed by Student's *t* test; * $p < 0.05$ and ** $p < 0.01$. Note that adhesion of HUVECs treated with MAGI-1 siRNAs to the VEC-Fc-coated dish was significantly reduced compared with mock-treated HUVECs. (B) Adhesion of MAGI-1-depleted cells to a collagen-coated dish was comparable to mock-treated HUVECs, as analyzed by the same method described in the legend for A. (C) HUVECs infected with either LacZ-expressing adenovirus (LacZ) or Rap1GAPII-expressing virus (Rap1GAP) were analyzed for adhesion to a VEC-Fc-coated dish similarly to A.

REFERENCES

Adamsky, K., Arnold, K., Sabanay, H., and Peles, E. (2003). Junctional protein MAGI-3 interacts with receptor tyrosine phosphatase beta (RPTP beta) and tyrosine-phosphorylated proteins. J. Cell Sci. *116*, 1279–1289.

Boettner, B., Govek, E. E., Cross, J., and Van Aelst, L. (2000). The junctional multidomain protein AF-6 is a binding partner of the Rap1A GTPase and associates with the actin cytoskeletal regulator profilin. Proc. Natl. Acad. Sci. USA *97*, 9064–9069.

Boettner, B., Harjes, P., Ishimaru, S., Heke, M., Fan, H. Q., Qin, Y., Van Aelst, L., and Gaul, U. (2003). The AF-6 homolog canoe acts as a Rap1 effector during dorsal closure of the *Drosophila* embryo. Genetics *165*, 159–169.

Bos, J. L. (2005). Linking Rap to cell adhesion. Curr. Opin. Cell Biol. *17*, 123–128.

Bos, J. L., de Rooij, J., and Reedquist, K. A. (2001). Rap1 signalling: adhering to new models. Nat. Rev. Mol. Cell Biol. *2*, 369–377.

Dejana, E. (2004). Endothelial cell-cell junctions: happy together. Nat. Rev. Mol. Cell Biol. *5*, 261–270.

Dobrosotskaya, I., Guy, R. K., and James, G. L. (1997). MAGI-1, a membrane-associated guanylate kinase with a unique arrangement of protein-protein interaction domains. J. Biol. Chem. *272*, 31589–31597.

Dobrosotskaya, I. Y. (2001). Identification of mNET1 as a candidate ligand for the first PDZ domain of MAGI-1. Biochem. Biophys. Res. Commun. *283*, 969–975.

Dobrosotskaya, I. Y., and James, G. L. (2000). MAGI-1 interacts with beta catenin and is associated with cell-cell adhesion structures. Biochem. Biophys. Res. Commun. *270*, 903–909.

Esser, S., Lampugnani, M. G., Corada, M., Dejana, E., and Risau, W. (1998). Vascular endothelial growth factor induces VE-cadherin tyrosine phosphorylation in endothelial cells. J. Cell Sci. *111*(Pt 13), 1853–1865.

Franke, B., Akkerman, J. W., and Bos, J. L. (1997). Rapid Ca2+-mediated activation of Rap1 in human platelets. EMBO J. *16*, 252–259.

Franklin, J. L., Yoshiura, K., Dempsey, P. J., Bogatcheva, G., Jeyakumar, L., Meise, K. S., Pearsall, R. S., Threadgill, D., and Coffey, R. J. (2005). Identification of MAGI-3 as a transforming growth factor-alpha tail binding protein. Exp. Cell Res. *303*, 457–470.

Fukuhara, S., Sakurai, A., Sano, H., Yamagishi, A., Somekawa, S., Takakura, N., Saito, Y., Kangawa, K., Mochizuki, N. (2005). Cyclic AMP potentiates vascular endothelial cadherin-mediated cell-cell contact to enhance endothelial barrier function through an Epac-Rap1 signaling pathway. Mol. Cell Biol. *25*, 136–146.

Fukuyama, T., Ogita, H., Kawakatsu, T., Fukuhara, T., Yamada, T., Sato, T., Shimizu, K., Nakamura, T., Matsuda, M., and Takai, Y. (2005). Involvement of the c-Src-Crk-C3G-Rap1 signaling in the nectin-induced activation of Cdc42 and formation of adherens junctions. J. Biol. Chem. *280*, 815–825.

Herren, B., Levkau, B., Raines, E. W., and Ross, R. (1998). Cleavage of beta-catenin and plakoglobin and shedding of VE-cadherin during endothelial apoptosis: evidence for a role for caspases and metalloproteinases. Mol. Biol. Cell *9*, 1589–1601.

Hirabayashi, S., Tajima, M., Yao, I., Nishimura, W., Mori, H., and Hata, Y. (2003). JAM4, a junctional cell adhesion molecule interacting with a tight junction protein, MAGI-1. Mol. Cell Biol. *23*, 4267–4282.

Hirao, K., Hata, Y., Ide, N., Takeuchi, M., Irie, M., Yao, I., Deguchi, M., Toyoda, A., Sudhof, T. C., and Takai, Y. (1998). A novel multiple PDZ domain-containing molecule interacting with N-methyl-D-aspartate receptors and neuronal cell adhesion proteins. J. Biol. Chem. *273*, 21105–21110.

Hirao, K., Hata, Y., Yao, I., Deguchi, M., Kawabe, H., Mizoguchi, A., and Takai, Y. (2000). Three isoforms of synaptic scaffolding molecule and their characterization. Multimerization between the isoforms and their interaction with N-methyl-D-aspartate receptors and SAP90/PSD-95-associated protein. J. Biol. Chem. *275*, 2966–2972.

Hogan, C., Serpente, N., Cogram, P., Hosking, C. R., Bialucha, C. U., Feller, S. M., Braga, V. M., Birchmeier, W., and Fujita, Y. (2004). Rap1 regulates the formation of E-cadherin-based cell-cell contacts. Mol. Cell Biol. *24*, 6690–6700.

Hudry-Clergeon, H., Stengel, D., Ninio, E., and Vilgrain, I. (2005). Platelet-activating factor increases VE-cadherin tyrosine phosphorylation in mouse endothelial cells and its association with the PtdIns3′-kinase. FASEB J. *19*, 512–520.

Hung, A. Y., and Sheng, M. (2002). PDZ domains: structural modules for protein complex assembly. J. Biol. Chem. *277*, 5699–5702.

Ide, N., Hata, Y., Deguchi, M., Hirao, K., Yao, I., and Takai, Y. (1999). Interaction of S-SCAM with neural plakophilin-related Armadillo-repeat protein/delta-catenin. Biochem. Biophys. Res. Commun. *256*, 456–461.

Iyer, S., Ferreri, D. M., DeCoco, N. C., Minnear, F. L., and Vincent, P. A. (2004). VE-cadherin-p120 interaction is required for maintenance of endothelial barrier function. Am. J. Physiol Lung Cell Mol. Physiol. *286*, L1143–L1153.

Kawajiri, A., Itoh, N., Fukata, M., Nakagawa, M., Yamaga, M., Iwamatsu, A., and Kaibuchi, K. (2000). Identification of a novel beta-catenin-interacting protein. Biochem. Biophys. Res. Commun. *273*, 712–717.

Knox, A. L., and Brown, N. H. (2002). Rap1 GTPase regulation of adherens junction positioning and cell adhesion. Science *295*, 1285–1288.

Kobielak, A., and Fuchs, E. (2004). Alpha-catenin: at the junction of intercellular adhesion and actin dynamics. Nat. Rev. Mol. Cell Biol. *5*, 614–625.

Kooistra, M. R., Corada, M., Dejana, E., and Bos, J. L. (2005). Epac1 regulates integrity of endothelial cell junctions through VE-cadherin. FEBS Lett. *579*, 4966–4972.

Kotelevets, L., van Hengel, J., Bruyneel, E., Mareel, M., van Roy, F., and Chastre, E. (2005). Implication of the MAGI-1b/PTEN signalosome in stabilization of adherens junctions and suppression of invasiveness. FASEB J. *19*, 115–117.

Laura, R. P., Ross, S., Koeppen, H., and Lasky, L. A. (2002). MAGI-1, a widely expressed, alternatively spliced tight junction protein. Exp. Cell Res. *275*, 155–170.

Mandell, K. J., Babbin, B. A., Nusrat, A., and Parkos, C. A. (2005). Junctional adhesion molecule 1 regulates epithelial cell morphology through effects on beta1 integrins and Rap1 activity. J. Biol. Chem. *280*, 11665–11674.

Mino, A., Ohtsuka, T., Inoue, E., and Takai, Y. (2000). Membrane-associated guanylate kinase with inverted orientation (MAGI)-1/brain angiogenesis inhibitor 1-associated protein (BAP1) as a scaffolding molecule for Rap small G protein GDP/GTP exchange protein at tight junctions. Genes Cells *5*, 1009–1016.

Mochizuki, N., Yamashita, S., Kurokawa, K., Ohba, Y., Nagai, T., Miyawaki, A., and Matsuda, M. (2001). Spatio-temporal images of growth-factor-induced activation of Ras and Rap1. Nature *411*, 1065–1068.

Nagashima, K., Endo, A., Ogita, H., Kawana, A., Yamagishi, A., Kitabatake, A., Matsuda, M., Mochizuki, N. (2002). Adaptor protein Crk is required for Ephrin-B1-induced membrane ruffling and focal complex assembly of human aortic endothelial cells. Mol. Biol. Cell *13*, 4231–4242.

Navarro, P., Ruco, L., and Dejana, E. (1998). Differential localization of VE- and N-cadherins in human endothelial cells: VE-cadherin competes with N-cadherin for junctional localization. J. Cell Biol. *140*, 1475–1484.

Nwariaku, F. E., Liu, Z., Zhu, X., Nahari, D., Ingle, C., Wu, R. F., Gu, Y., Sarosi, G., and Terada, L. S. (2004). NADPH oxidase mediates vascular endothelial cadherin phosphorylation and endothelial dysfunction. Blood *104*, 3214–3220.

Ohba, Y. *et al.* (2001). Requirement for C3G-dependent Rap1 activation for cell adhesion and embryogenesis. EMBO J. *20*, 3333–3341.

Price, L. S., Hajdo-Milasinovic, A., Zhao, J., Zwartkruis, F. J., Collard, J. G., and Bos, J. L. (2004). Rap1 regulates E-cadherin-mediated cell-cell adhesion. J. Biol. Chem. *279*, 35127–35132.

Subauste, M. C., Nalbant, P., Adamson, E. D., and Hahn, K. M. (2005). Vinculin controls PTEN protein level by maintaining the interaction of the adherens junction protein beta-catenin with the scaffolding protein MAGI-2. J. Biol. Chem. *280*, 5676–5681.

Tachibana, K., Nakanishi, H., Mandai, K., Ozaki, K., Ikeda, W., Yamamoto, Y., Nagafuchi, A., Tsukita, S., and Takai, Y. (2000). Two cell adhesion molecules, nectin and cadherin, interact through their cytoplasmic domain-associated proteins. J. Cell Biol. *150*, 1161–1176.

Tanaka, Y., Nakanishi, H., Kakunaga, S., Okabe, N., Kawakatsu, T., Shimizu, K., and Takai, Y. (2003). Role of nectin in formation of E-cadherin-based adherens junctions in keratinocytes: analysis with the N-cadherin dominant negative mutant. Mol. Biol. Cell *14*, 1597–1609.

Volberg, T., Geiger, B., Kartenbeck, J., and Franke, W. W. (1986). Changes in membrane-microfilament interaction in intercellular adherens junctions upon removal of extracellular Ca2+ ions. J. Cell Biol. *102*, 1832–1842.

Wittchen, E. S., Worthylake, R. A., Kelly, P., Casey, P. J., Quilliam, L. A., and Burridge, K. (2005). Rap1 GTPase inhibits leukocyte transmigration by promoting endothelial barrier function. J. Biol. Chem. *280*, 11675–11682.

Yamada, A., Irie, K., Hirota, T., Ooshio, T., Fukuhara, A., and Takai, Y. (2005). Involvement of the annexin II-S100A10 complex in the formation of E-cadherin-based adherens junctions in Madin-Darby canine kidney cells. J. Biol. Chem. *280*, 6016–6027.

Zanetti, A., Lampugnani, M. G., Balconi, G., Breviario, F., Corada, M., Lanfrancone, L., and Dejana, E. (2002). Vascular endothelial growth factor induces SHC association with vascular endothelial cadherin: a potential feedback mechanism to control vascular endothelial growth factor receptor-2 signaling. Arterioscler. Thromb. Vasc. Biol. *22*, 617–622.

Available online at www.sciencedirect.com
SCIENCE DIRECT®
Cellular Signalling xx (2005) xxx–xxx
CELLULAR SIGNALLING
www.elsevier.com/locate/cellsig

ERK is an anti-inflammatory signal that suppresses expression of NF-κB-dependent inflammatory genes by inhibiting IKK activity in endothelial cells

Yong-Sun Maeng [a,1], Jeong-Ki Min [a,1], Jeong-Hun Kim [b], Akiko Yamagishi [c], Naoki Mochizuki [c], Ja-Young Kwon [d], Yong-Won Park [d], Young-Myeong Kim [e], Young-Guen Kwon [a,*]

[a] *Department of Biochemistry College of Sciences, Yonsei University, Seoul 120-749, Korea*
[b] *Department of Ophthalmology Seoul National University College of Medicine, Seoul Artificial Eye Center, Clinical Research Institute, Seoul National University Hospital, Seoul 110-744, Korea*
[c] *Department of Structural Analysis, National Cardiovascular Center Research Institute, 5-7-1 Fujishirodai, Suita, Osaka 565-8565, Japan*
[d] *Department of Obstetrics and Gynecology Yonsei University College of Medicine 134 Shinchon-dong, Seodaemoon-gu Seoul 120-752, Korea*
[e] *Department of Molecular and Cellular Biochemistry, School of Medicine, Kangwon National University, Chunchon, Kangwon-Do 200-701, Korea*

Received 29 July 2005; received in revised form 20 August 2005; accepted 22 August 2005

Abstract

Unveiling of endothelial nuclear factor-κB (NF-κB) activation is pivotal for understanding the inflammatory reaction and the pathogenesis of inflammatory vascular diseases. We here report the novel function of extracellular signal-related kinase (ERK) in controlling endothelial NF-κB activation and inflammatory responses. In human endothelial cells, vascular endothelial growth factor (VEGF) induced NF-κB-dependent transcription of cell adhesion molecules (CAMs) and monocyte adhesion. These effects were prominently enhanced by either pretreatment with the MEK inhibitors, PD98059 and U0126 or overexpression of a dominant negative form of MEK, but blocked by a wild type ERK. Consistently, inhibition of ERK significantly increased IκB kinase (IKK) activity, IκBα phosphorylation, and nuclear translocation of NF-κB induced by VEGF, whereas overexpression of ERK resulted in the loss of these responses to VEGF. Using two PKC inhibitors has demonstrated that VEGF concomitantly stimulates IKK and its negative regulatory signal ERK through PKC that lies downstream of KDR/Flk. Strikingly, elevation of ERK in endothelial cells markedly inhibited CAM expression and NF-κB activation as well as monocyte adhesion induced by IL-1β and TNF-α. The data collectively suggest that ERK serves as an anti-inflammatory signal that suppresses expression of NF-κB-dependent inflammatory genes by inhibiting IKK activity in endothelial cells. Measuring the existence of ERK activity in vascular endothelial cells may be useful for predicting the feasibility and potency of inflammatory reactions in the vasculature.

Keywords: VEGF; ERK; NF-κB; CAMs; Inflammation

1. Introduction

Inflammatory conditions are characterized by the migration of proliferating leucocytes from the blood to the tissues and involve a coordinated series of adhesion processes between circulating and resident leukocytes and the vascular endothelium [1–3]. These events are controlled by different types of adhesion molecules on the leukocytes and endothelium [3]. In particular, expression of cell adhesion molecules (CAMs), such as E-selectin, intercellular adhesion molecule-1 (ICAM-1), and vascular cell adhesion molecule-1 (VCAM-1),

Abbreviations: VEGF, vascular endothelial growth factor; HUVECs, human umbilical vein endothelial cells; bFGF, basic fibroblast growth factor; EGF, epidermal growth factor; TNF-α, tumor necrosis factor-α; IL-1β, interleukin-1β; KDR, Flk-1/kinase-insert domain containing receptor; VCAM-1, vascular cell adhesion molecule-1; ICAM-1, intercellular adhesion molecule-1; PI3K, phosphatidylinositol 3′-kinase; PLC, phospholipase C; PKC, protein kinase C; IKK, IκB kinase; MEK, mitogen-activated protein/extracellular signal-regulated kinase kinase; ERK, extracellular signal-regulated kinase; RT-PCR, reverse transcriptase-polymerase chain reaction.

* Corresponding author. Tel.: +82 2 2123 5697; fax: +82 2 362 9897.
E-mail address: ygkwon@yonsei.ac.kr (Y.-G. Kwon).
[1] These authors contributed equally to this study.

0898-6568/$ - see front matter © 2005 Elsevier B.V. All rights reserved.
doi:10.1016/j.cellsig.2005.08.007

on the surface of endothelial cells is required for endothelial–leukocyte cell interaction [1]. In the absence of inflammation, CAM expression is low on the endothelial cells of most vascular beds, but it dramatically increases in response to a number of extracellular stimuli, including tumor necrosis factor-α (TNF-α), interleukin-1β (IL-1β), vascular endothelial growth factor (VEGF), and bacterial lipopolysaccharides [4–6]. Among the classical transcription factors activated by inflammatory cytokines, nuclear factor-κB (NF-κB) plays a pivotal role in the regulation of inflammatory response genes [7,8]. Indeed, it is considered to be a major transcriptional regulator of CAMs in endothelial cells [9].

In mammalian, the five members of the NF-κB family, p65 (RelA), RelB, c-Rel, p50/p105 (NF-κB1), and p52/p100 (NF-κB2), exist in quiescent cells as homo- or heterodimers bound to IκB family proteins and retained in the cytoplasm as an inactive state [10]. In stimulated cells, IκB is degraded through the ubiquitin-proteasome pathway upon specific phosphorylation by activated IκB kinase (IKK) [11]. The IKK activity in cells can be purified as a 700–900-kDa complex, and has been shown to contain two kinase subunits, IKKα (IKK1) and IKKβ (IKK2), and a regulatory subunit, NEMO (NF-κB essential modifier) or IKKγ [11–13]. In the canonical NF-κB signaling pathway, IKKβ is both necessary and sufficient for phosphorylation of IκBα on Ser 32 and Ser 36, and IκBβ on Ser 19 and Ser 23 [12]. By contrast, although the role of IKKα in the canonical pathway is unclear, recent studies suggest that the IKKα subunit phosphorylates p100 and causes its inducible processing to p52 [13].

The activation of the IKK complex is suggested to be exerted by phosphorylation of the IKK complex by the mitogen-activated protein kinase kinase kinase (MAP3K) family including NF-κB-inducing kinase [14], mitogen-activated protein/ERK kinase kinase 1 (MEKK) [15], MEKK3 [16], TGF-β activating kinase 1 [17] and NF-κB-activating kinase [18]. The MAP3K family phosphorylated and induced NF-κB activation when overexpressed or when assayed in vitro, but the mechanism by which cytokines lead to the activation of the IKK complex in vivo is still controversial [19]. Alternatively, previous studies have also suggested that IKK recruitment to receptor complexes at the cell membrane results in its autophosphorylation and subsequent activation [20]. Indeed, IKK recruitment to the TNF receptor-1 complex is shown to be required for TNFα-mediated activation of the IKK complex [11,21–23]. In addition, the important involvement of various intracellular adaptors such as TNF-receptor-associated factors and death-domain kinase receptor-interacting protein in receptor-mediated NF-κB pathway has been extensively reported [24]. However, despite of a large number of studies in vitro and in vivo, the specific upstream signaling mechanism that regulates the IKK activity remains for further investigation.

In the present study, we report an important regulatory role of extracellular signal-related kinase (ERK) in controlling expression of NF-κB-dependent inflammatory genes in vascular endothelial cells. We found that inhibition of ERK markedly increased CAM expression in response to VEGF, which induces both ERK and NF-κB activation in endothelial cells, and this effect was correlated with increased NF-κB activation. Furthermore, elevation of ERK activity in endothelial cells resulted in the suppression of CAM expression and NF-κB activation as well as leukocyte adhesion induced by IL-1β and TNF-α in addition to VEGF. We therefore propose that ERK is a potential intracellular regulator that suppresses vascular inflammation by inhibiting NF-κB activation in endothelial cells.

2. Materials and methods

2.1. Cell culture and reagents

Human umbilical vein endothelial cells (HUVECs) were isolated from human umbilical cord veins by collagenase treatment as described previously [25] and used in passages 2–7. The cells were grown in M199 medium (Invitrogen, Carlsbad, CA) supplemented with 20% fetal bovine serum, 100 units/ml penicillin, 100 G μ/ml streptomycin, 3 ng/ml bFGF (Upstate Biotechnology, Lake Placid, NY), and 5 units/ml heparin at 37 °C in humidified 5% CO2/95% air. U937 cells were grown in RPMI-1640 (Invitrogen). VEGF was from Upstate Biotechnology (Lake Placid, NY), PD98059 from Alexis (San Diego, CA), and U0126 and GF109203X from BIOMOL (Plymouth Meeting, PA). Chelerythrine chloride and actinomycin D were from Sigma. M199, heparin, Trizol reagent and LipofectAMINE Plus were purchased from Invitrogen. Antibodies used were as follows: rabbit anti-VCAM-1 polyclonal antibody, mouse anti-actin monoclonal antibody (Santa Cruz Biotechnology, SantaCruz, Calif), rabbit anti-phospho-IκB-α polyclonal antibody (Cell Signaling, Beverly, MA), mouse anti-phospho-ERK (Thr-202/Tyr-204) monoclonal antibody, and rabbit anti-ERK polyclonal antibody (New England Biolabs, Beverly, MA). All other reagents were purchased from Sigma unless otherwise indicated.

2.2. Construction of reporter plasmids

The VCAM-1 luciferase plasmids were constructed as described previously [26]. The human VCAM-1 promoter, spanning 1716 to +119 bp, was amplified by PCR with primers containing 5′ *KpnI* and 3′ *Xho*I restriction sites. The resulting PCR fragment was digested with *Kpn*I and *Xho*I and cloned into pGL3-basic vector (Promega). Synthetic oligonucleotide sense and antisense primers were used to generate a series of DNA fragments with successive 5′ deletions. All PCR products were digested with *KpnI* and *XhoI* and cloned into pGL3-basic vector. The following deletion constructs of the human VCAM-1 promoter were generated: 1716 to +119 bp (fragment 6), 366 to +119 bp (fragment 5), 296 to +119 bp (fragment 4), 210 to +119 bp fragment 3) and 38 to +119 bp (fragment 2). To construct the ICAM-1 luciferase plasmid, we cloned regions spanning −1350 to +45 bp of the human ICAM-1 promoter into pGL3-basic vector (Promega). Plasmid DNAs were purified from bacterial cultures using an Endofree Plasmid Maxi kit (Qiagen, Chatsworth, CA). We confirmed all constructs by restriction enzyme mapping and sequencing.

2.3. Transfections and analysis of luciferase activity

HUVECs were transfected with 1 μg of the above plasmids and 1 μg of the control pCMV-β-gal plasmid using LipofectAMINE Plus reagents (Invitrogen, Carlsbad, CA). Cell extracts were prepared twenty-four hours after transfection, and luciferase assays carried out with the Luciferase Assay System (Promega). Luciferase activities were normalized with respect to parallel β-galactosidase activities, to correct for differences in transfection efficiency, and the β-galactosidase assays were performed using the β-Galactosidase Enzyme Assay System (Promega). Each experimental point was performed in at least quadruplicate.

2.4. Flow cytometry

Cells from subconfluent cultures were detached gently from plates with PBS containing 2 mM EDTA. The cells were washed two or three times with PBS, resuspended in PBS containing 3% bovine serum albumin and incubated with FITC-conjugated VCAM-1 antibody (Serotec) for 30 min on ice. They were then fixed with 2% paraformaldehyde and analyzed by flow cytometry in a fluorescence-activated cell sorter (Becton Dickinson). Each experimental condition was performed in quadruplicate.

2.5. Semi-quantitative RT-PCR analysis

Total RNA was obtained from HUVECs with a TRIzol reagent kit. 0.5–5 μg RNA samples were used in the reverse transcriptase-polymerase chain reactions (RT-PCR), and the correlation between the amounts of RNA used and quantity of PCR products from VCAM-1 mRNA and the internal standard (β-actin) mRNA was examined. Briefly, target RNA was converted to cDNA by treatment with 200 units of reverse transcriptase and 500 ng of oligo(dT) primer in 50 mM Tris–HCl (pH 8.3), 75 mM KCl, 3 mM $MgCl_2$, 10 mM dithiothreitol, and 1 mM dNTPs at 42 °C for 1 h. The reaction was stopped by heating at 70 °C for 15 min. One μl of the cDNA mixture was used for enzymatic amplification. The polymerase chain reaction was performed in 50 mM KCl, 10 mM Tris–HCl (pH 8.3), 1.5 mM $MgCl_2$, 0.2 mM dNTPs, 2.5 units of *Taq* DNA polymerase, and 0.1 μM of primers for VCAM-1. Amplification was performed in a DNA thermal cycler (model PTC-200; MJ Research) under the following condition: denaturation at 94 °C for 5 min for the first cycle and for 30 s thereafter, annealing at 60 °C (VCAM-1), for 30 s, and extension at 72 °C for 30 s for 25 repetitive cycles. Final extension was at 72 °C for 10 min. The primers used for VCAM-1 were as follows: 5′-GATACAACCGTCTTGGTCAGCCC-3′ (sense) and 5′CGC-ATCCTTCAACTGGCCTT-3′ (antisense). Each experimental condition was performed in quadruplicate.

2.6. Transfer vector constructs

HIV-vectors were produced from the previously described SIN-18 vector, which contains a large deletion in the U3 region of the 3′ long terminal repeat (LTR) [27]. The SIN.cPPT.CMV-EGFP-W vector contained the enhanced green fluorescent protein (EGFP) transgene driven by the human cytomegalovirus (CMV) immediate-early enhancer/promoter. The SIN.cPPT.ERK2-EGFP-W vector contained the human extracellular signal-related kinase 2 gene.

2.7. Lentiviral vectors and in vitro gene transfer

VSV-G-pseudotyped, HIV-1-based vector particles were produced by cotransfection of four plasmids (pMDLg/pRRE: 12 μg; pRSVrev: 3 μg; pMD.G: 5 μg, SIN vector: 20 μg) onto 293T cells. Culture medium was replaced by serum-free SFM-II medium (Invitrogen) 15 h post-transfection. Thirty-two hours later, cell supernatants were harvested, filtered through a 0.45 μm filtration system, concentrated on Centricon Plus-80 Biomax MW 100,000 (Millipore, Le-Mont-sur-Lausanne, Switzerland), resuspended in PBS, and re-concentrated on Centricon-20. The titer of the SIN.cPPT.CMV-EGFP-W vector stock solution was 5×10^9 transducing units (TU)/ml by flow cytometry on 293T cells, and 3×10^4 ng p24 antigen per ml by p24-ELISA. The SIN.cPPT.ERK2-EGFP-W vector was titered by flow cytometry on HUVECs (of note, titration of SIN.cPPT.CMV-EGFP-W yielded similar results in HUVECs and 293T cells). HUVECs were seeded in six-well plates and allowed to adhere overnight. Viral vectors were added to cell cultures at varying multiplicities of infection (MOIs ≈1–50). At 18 h, cells were washed and medium was replaced. Cells were harvested at the indicated time points. Percentages of EGFP-positive cells and their mean fluorescence values (MFVs) were determined by flow cytometry (FACScan).

2.8. Preparation of nuclear extracts and electrophoretic mobility shift assays

Cells were washed three times with ice-cold Tris-buffered saline (TBS) and resuspended in 400 μl of buffer A [10 mM HEPES (pH 7.9), 10 mM KCl, 0.1 mM EDTA, 0.1 mM EGTA, 1 mM dithiothreitol (DTT), 1 mM phenylmethylsulfonyl fluoride (PMSF), 5 μg/mL of leupeptin, and 5 μg/mL of aprotinin]. After 15 min, Nonidet P-40 (NP-40) was added to a final concentration of 0.6%. Nuclei were pelleted and suspended in 50 μl of buffer C [20 mM HEPES (pH 7.9), 0.4 M NaCl, 1 mM EDTA, 1 mM EGTA, 1 mM DTT, 1 mM PMSF, 5 μg/ml of leupeptin, and 5 μg/ml of aprotonin]. After 30 min agitation at 4 °C, the lysates were centrifuged, and the supernatants containing the nuclear proteins were diluted with buffer C. Binding reactions contained 15 μg of nuclear protein and a ^{32}P end-labeled, double-stranded oligonucleotide containing the NF-κB binding site on the human VCAM-1 promoter (5′-CCTTGAAGGGATTTCCCTCC-3′) and were incubated for 30 min. Cold competition controls were performed by preincubating the nuclear proteins with a 20-fold molar excess of unlabeled NF-κB double-stranded oligonucleotide for 20 min. The mixtures were resolved on native 5% polyacrylamide gels, which were dried and autoradiographed.

Each experimental point was performed in duplicate and represents several independent conditions.

2.9. In vitro kinase assays

IKK was assayed as described previously [28]. Briefly, the IKK complex was precipitated from whole cell extracts with antibody against IKK-γ, followed by treatment with protein A-Sepharose beads (Pierce). After a 2 h incubation, the beads were washed with lysis buffer and assayed in kinase assay mixture containing 50 mM HEPES (pH 7.4), 20 mM $MgCl_2$, 2 mM dithiothreitol, 20 Ci μof [γ-^{32}P]ATP, 10 μM unlabeled ATP, and 2 μg of substrate GST-IκBα (amino acids 1–54). After incubation at 30 °C for 30 min, the reaction was terminated by boiling in SDS sample buffer for 5 min. Finally, the protein was resolved on 10% SDS-PAGE, the gel was dried, and the radioactive bands were visualized with a PhosphorImager. To determine the total amounts of IKK complex in each sample, 50 μg of whole cell protein was resolved on 7.5% SDS-PAGE, electrotransferred to a nitrocellulose membrane, and blotted with anti-IKK-γ antibody. The data represent the average of two separate experiments, each performed in duplicate.

2.10. Immunocytochemical localization of p65

Nuclear translocation of the p65 subunit of NF-κB was examined by an immunocytochemical method as described previously [28]. Briefly, treated cells were fixed with 2% paraformaldehyde and permeabilized with 0.2% Triton X-100. After washing in phosphate-buffered saline, the slides were blocked with 3% bovine serum albumin for 1 h and the cells incubated with goat polyclonal anti-p65 antibody (Santa Cruz

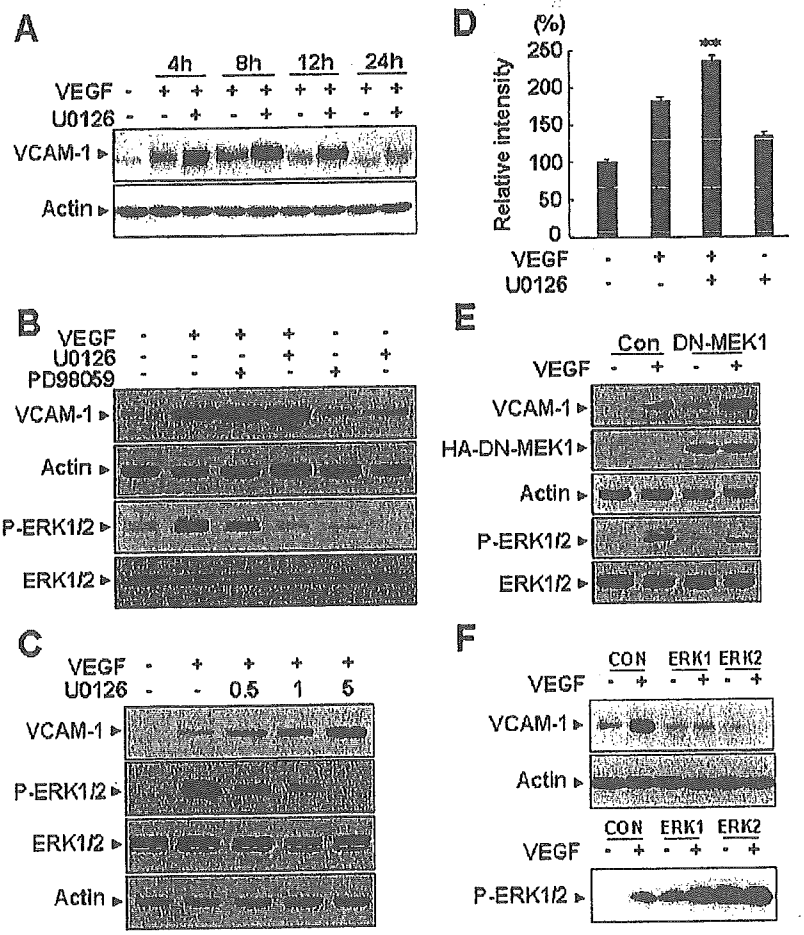

Fig. 1. Inhibition of ERK resulted in increased expression of VCAM-1 in response to VEGF. (A) HUVECs were incubated for 30 min with or without 5 μM U0126 and stimulated with 10 ng/ml VEGF for the indicated times. (B) HUVECs were pretreated for 30 min with 5 μM U0126 or 10 μM PD98059 prior to stimulation with 10 ng/ml VEGF for 10 min (*lower panel*) or 8 h (*upper panel*). (C) HUVECs were incubated for 30 min with or without various concentrations of U0126 and stimulated with 10 ng/ml VEGF for 10 min (*lower panel*) or 8 h (*upper panel*). Western blots were probed with anti-VCAM-1 antibody and an anti-phospho-ERK antibody, and reprobed with anti-actin antibody or anti-ERK antibody to verify equal loading of proteins. (D) HUVECs were pretreated for 30 min with 5 μM U0126 and then stimulated with 10 ng/ml VEGF for 8 h. The cells were detached from the plates, treated with FITC-conjugated VCAM-1 antibody and analyzed with a FACScan. Staining was quantified by flow cytometry. HUVECs were transfected with hemagglutinin (HA) tagged dominant negative form of MEK1, DN-MEK1, (E) or a wild form of ERKs (ERK1, 2) (F) and then stimulated with VEGF (10 ng/ml) for 10 min (*lower panel*) or 8 h (*upper panel*). Western blots were probed with anti-VCAM-1, anti-HA, and anti-phospho-ERK antibody and reprobed with anti-actin antibody or anti-ERK antibody to verify equal loading of proteins. Con indicates cells transfected with empty vector. **, $P<0.01$ versus VEGF alone.

Biotechnology, Santa Cruz, CA) (1:100). After 2 h at 4 °C the cells were washed and incubated with anti-goat IgG-rhodamine (Santa Cruz) (1:100) for 1 h. The cells were then mounted with mounting medium and observed with a fluorescence microscope (Olympus).

2.11. Adhesion assays

HUVECs were plated on 2% gelatin-coated 96-well plates at a density of 1×10^4 cells/well and stimulated with VEGF for 8 h. Human U937 cells were then added (5×10^4 cells/ml, 200 μl/well) to the confluent HUVEC monolayers and incubated for 30 min. Thereafter the cells in the wells were washed out 3 times with PBS, fixed and stained with Diff-Quick (Baxter Healthcare Corp., McGraw Park, IL). The adherent cells in 5 randomly selected optical fields of each well were counted. Each experimental point was performed in duplicate and represents several independent conditions.

2.12. Western blotting

Cell lysates or immunoprecipitates were fractionated by SDS-PAGE and transferred to polyvinyldifluoride membranes. The blocked membranes were incubated with the appropriate antibody, and the immunoreactive bands were visualized with a

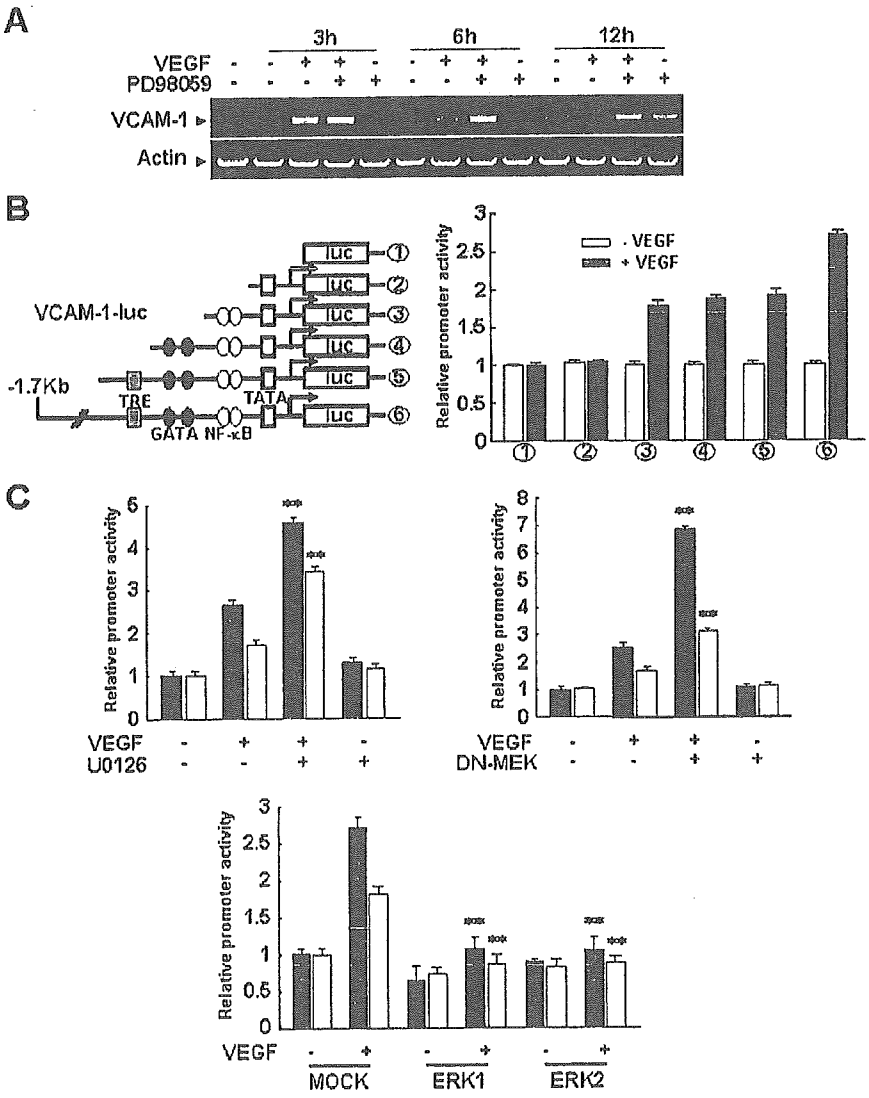

Fig. 2. ERK down-regulates VEGF-induced transcription of VCAM-1 by inhibiting NF-κB. (A) HUVECs were incubated for 30 min with or without 10 μM PD98059 and stimulated with 10 ng/ml VEGF for the indicated times. Total mRNAs were isolated and RT-PCR was performed with specific primers for human VCAM-1 as described in "Materials and methods". Actin served as an internal control. (B) HUVECs were cotransfected with a β-galactosidase plasmid and the various pVCAM-1-Luc deletion constructs as depicted. Twenty four hours later they were stimulated with 10 ng/ml VEGF for 24 h. (C) HUVECs were cotransfected with pVCAM-1-Luc (fragment 6: 1.8 kilobase pair, fragment 3: 329 bp), a β-galactosidase plasmid, and a dominant negative form of MEK1 (DN-MEK1), or wild form of ERKs (ERK1, 2). Twenty four hours after transfection, they were incubated with 10 ng/ml VEGF for 24 h. Luciferase activity was normalized to β-galactosidase activity. Data are means ±S.D. of luciferase light units relative to control untreated cells (set at 100%) in quadruplicate experiments. **, $P<0.01$ versus VEGF alone or MOCK+VEGF.

chemiluminescent reagent as recommended by Amersham Biosciences, Inc.

2.13. Statistical analysis

Data are presented as means±S.E, and statistical comparisons between groups were performed by 1-way ANOVA followed by Student's *t* test.

3. Results

3.1. Inhibition of ERK resulted in increased expression of VCAM-1 in response to VEGF

Vascular endothelial growth factor (VEGF), a well characterized angiogenic factor, also acts as a proinflammatory cytokine that produces enhanced leukocyte rolling and adhesion and increases endothelial permeability [29,30]. In endothelial cells, it strongly activates ERK and also induces expression of CAMs [31,32] in a NF-κB-dependent mechanism [31]. However, the level of CAM induction in response to VEGF is significantly lower, when compared in parallel, than those by TNF-α and IL-β, which show very little or negligible effect on ERK activation in endothelial cells (data not shown). Thus, it is supposed that the ERK pathway may interfere expression of inflammatory CAMs in response to proinflammatory factors in endothelium. To test this possibility, we first evaluated the role of ERK in VEGF-induced expression of inflammatory response gene such as VCAM-1 by employing MEK inhibitors, PD98059 and U0126, in endothelial cells. Treatment of HUVECs with VEGF enhanced VCAM-1 expression, with a maximum at 8 h (Fig. 1A). In the presence of 5 μM U0126, the effect of VEGF was markedly increased and prolonged up to 24 h (Fig. 1A). To confirm this inhibitory effect, we treated HUVECs with VEGF

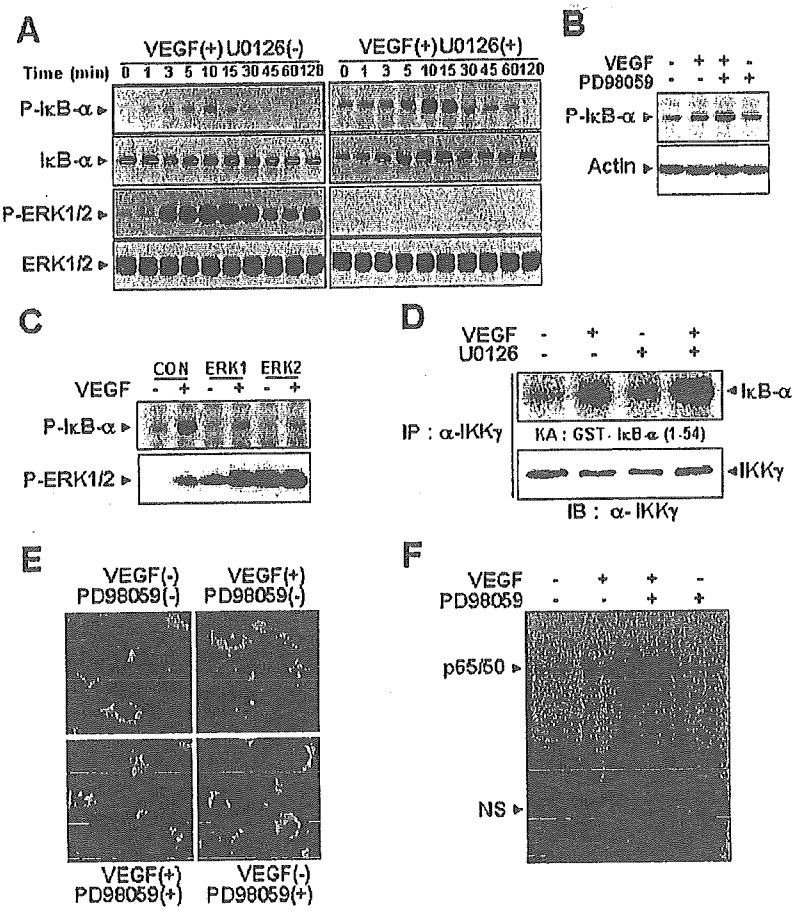

Fig. 3. Inhibition of ERK increases VEGF-induced IKK activity and nuclear translocation of NF-κB. (A) HUVECs were preincubated for 30 min with or without 5 μM U0126 and then stimulated with 10 ng/ml VEGF for the indicated times. Western blots were probed with anti-phospho-IκBα, anti-IκBα, anti-phospho-ERK, and anti-ERK antibodies. (B) HUVECs were preincubated for 30 min with or without 10 μM PD98059 and then stimulated with 10 ng/ml VEGF for 10 min. Western blots were probed with anti-phospho-IκBα and reprobed with an anti-actin antibody to verify equal loading of protein in each. (C) HUVECs were transfected with ERKs wild form (ERK1, 2) and then stimulated with VEGF for 10 min. Western blots were probed with anti-phospho-IκBα, and anti-phospho-ERK antibodies. (D) IKK activity was assessed by immune complex kinase assay as described in "Materials and methods". Recovery of IKK was assessed by immunoblotting for IKK-γ. (E) Immunocytochemical analysis of p65 localization. HUVECs were preincubated for 30 min with or without 10 μM PD98059 and then stimulated with 10 ng/ml VEGF for 30 min and subjected to immunocytochemistry as described in "Materials and methods". (F) HUVECs were preincubated for 30 min with or without 10 μM PD98059 and then stimulated with VEGF (20 ng/ml) for 30 min. Nuclear extracts were isolated and gel shift assay performed with a ^{32}P-radiolabeled NF-κB oligonucleotide of human VCAM-1.

for 10 min in the presence or absence of 5 μM U0126 and measured ERK activity by Western blotting with antibody against the phosphorylated form of ERK1/2 (p44 ERK1 and p42 ERK2). As shown in Fig. 1B, U0126 completely inhibited VEGF-induced ERK activation, whereas VEGF-induced VCAM-1 expression was increased (Fig. 1B). Pretreatment with the other MEK inhibitor, PD98059, also augmented VEGF-induced VCAM-1 expression, while reducing ERK activation (Fig. 1B). U0126 or PD98059 alone had no effect on VCAM-1 expression (Fig. 1B). In addition, the U0126-induced increase in VEGF-induced VCAM-1 expression was dose-dependent, and inversely related to ERK activity (Fig. 1C). FACScan analysis confirmed that U0126 augmented VEGF-induced expression of VCAM-1 on the cell surface of HUVECs (Fig. 1D).

To further confirm that the enhancement of VEGF-induced VCAM-1 expression by the inhibitors was due specifically to inhibition of ERK signaling, we determined the effects of a dominant negative MEK1 (DN-MEK1) mutant and two types of wild type ERK (ERK1 and ERK2). In agreement with the results with chemical inhibitors, Western blot analysis showed that overexpression of DN-MEK1 reduced VEGF-induced ERK phosphorylation, and increased the induction of VCAM-1 by VEGF (Fig. 1E). Moreover, there was a small increase in basal VCAM-1 expression in the cells expressing DN-MEK-1 (Fig. 1E). In contrast, HUVECs overexpressed with either wild type ERK1 or ERK2 increased ERK phosphorylation, and decreased VCAM-1 expression in response to VEGF (Fig. 1F). These results confirm that the ERK pathway inhibits VEGF signaling leading to VCAM-1 expression in endothelial cells.

3.2. ERK down-regulates VEGF-induced transcription of VCAM-1 by inhibiting NF-κB

To determine whether ERK inhibits VEGF-activated transcription of VCAM-1 in endothelial cells, we performed semi-quantitative RT-PCR and assayed transcription from the VCAM-1 luciferase plasmids described in Materials and methods. Treatment of HUVECs with VEGF in the absence of ERK inhibitor induced the appearance of VCAM-1 mRNA within 3 h, and the mRNA declined thereafter (Fig. 2A). In the presence of 10 μM PD98059, the level of VCAM-1 mRNA induced by VEGF was increased and sustained up to 12 h (Fig. 2A). These changes could result either from new synthesis or from increased mRNA stability. Pretreatment with actinomycin D, an inhibitor of transcription, almost completely prevented the increase of VCAM-1 mRNA in response to PD98059 (data not shown), suggesting that ERK inhibits VEGF-activated transcription. The human VCAM-1 promoter (1.7 kb) includes binding sites for NF-κB, TRE, and GATA [26]. Although previous report have implicated NF-κB in VEGF-induced VCAM-1 expression in endothelial cells [26,33], its precise role in activation of the VCAM-1 promoter has not been determined. To identify the cis elements involved, we serially deleted the 1.7 kb VCAM-1 promoter and introduced the resulting plasmids into HUVECs. As shown in Fig. 2B, deletion of the 5′ 1.2 kb region substantially reduced the response to VEGF, but further deletion of the TRE and GATA sites had no appreciable effect. Deletion of the proximal NF-κB binding sites located about 65 and 75 bp upstream of the transcription start site resulted in complete lose of responsiveness to VEGF. These results demonstrate that the NF-κB motifs on the VCAM-1 promoter are important for VEGF-mediated activation of the VCAM-1 promoter, together with an unidentified element in the 5′ 1.2 kb upstream region.

To further confirm the role of ERK in VEGF-induced VCAM-1 transcription, HUVECs were transiently transfected with a VCAM-1 luciferase plasmid harboring the VCAM-1 promoter region. As shown in Fig. 2C, VEGF induced VCAM-1-dependent transcriptional activity, and this was increased by pretreatment with 5 μM U0126, or by introducing DN-MEK-1, but abrogated by ERK or ERK2. These results confirm that ERK controls VEGF-mediated expression of VCAM-1 at the transcriptional level. Since the NF-κB motifs play a significant role in VEGF-induced transcription of VCAM-1, it seemed possible that ERK suppressed activation of NF-κB by VEGF. Indeed, VEGF-induced transcription from a luciferase plasmid containing the proximal NF-κB binding sites of the VCAM-1 promoter was markedly increased by U0126 and DN-MEK1, and almost completely blocked by ERK1 or ERK2 (Fig. 2C). These results suggest that ERK inhibits VEGF-induced transcription of VCAM-1 mRNAs at least in part by suppressing transcription from the NF-κB elements in the VCAM-1 promoter.

3.3. Inhibition of ERK increases VEGF-induced IKK activity and nuclear translocation of NF-κB

The activated form of NF-κB is a heterodimer that usually consists of two proteins, a p65 (also called relA) subunit and a

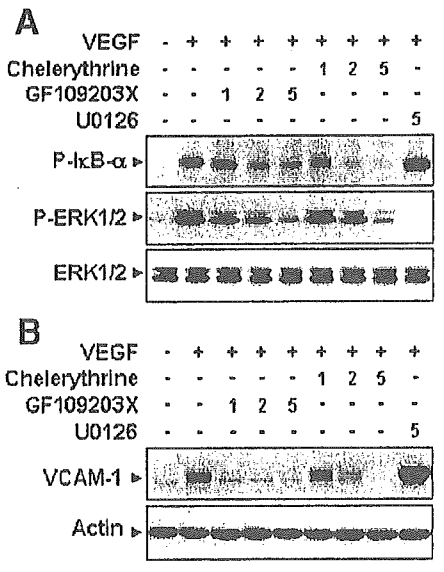

Fig. 4. PKC mediates both IκBα phosphorylation and ERK activation by VEGF. HUVECs were preincubated for 30 min with or without GF109203X, chelerythrine chloride (1, 2, or 5 μM) or 5 μM U0126 and then stimulated with 10 ng/ml VEGF for 10 min (A) or 8 h. (B). Western blots were probed with anti-phospho-IκBα, anti-IκBα, anti-phospho-ERK, and anti-ERK antibodies (A), and anti-VCAM-1 and anti-actin antibodies (B). Actin was used to verify equal loading of protein.

p50 subunit [7]. In the inactive state, NF-κB is found in the cytoplasm bound to IκBα, which prevents it from entering the nuclei [7,34]. Activation of NF-κB is preceded by the phosphorylation, ubiquitination, and proteolytic degradation of IκBα [34]. Therefore, we examined the effect of ERK inhibitors on VEGF-induced IκBα phosphorylation and degradation by Western blotting with antibodies against phospho-IκBα (Ser-32) and IκBα. As shown in Fig. 3A, VEGF treatment led to phosphorylation of IκBα and maximal activation was observed after 10 min. Pretreatment with U0126 substantially enhanced VEGF-induced IκBα phosphorylation. Moreover, while degradation of IκBα was barely detectable after stimulation with VEGF on its own, when U0126 was added, the level of IκBα markedly decreased following 30 min of VEGF treatment (Fig. 3A). We also observed that PD98059 increased the effect of VEGF on phosphorylation and subsequent degradation of IκBα in a manner similar to U0126 (Fig. 3B). In contrast, VEGF-induced IκBα phosphorylation was almost completely abrogated by overexpression of ERK1 or ERK2 (Fig. 3C). To further confirm the effect of U0126 on VEGF-induced IκBα phosphorylation, the IκB kinase (IKK) enzymatic assay was performed. IKK is a complex composed of three subunits: IKKα (IKK1), IKKβ (IKK2), and IKKγ (NEMO, IKKAP) [11]. IKK activity was determined in anti-IKKγ

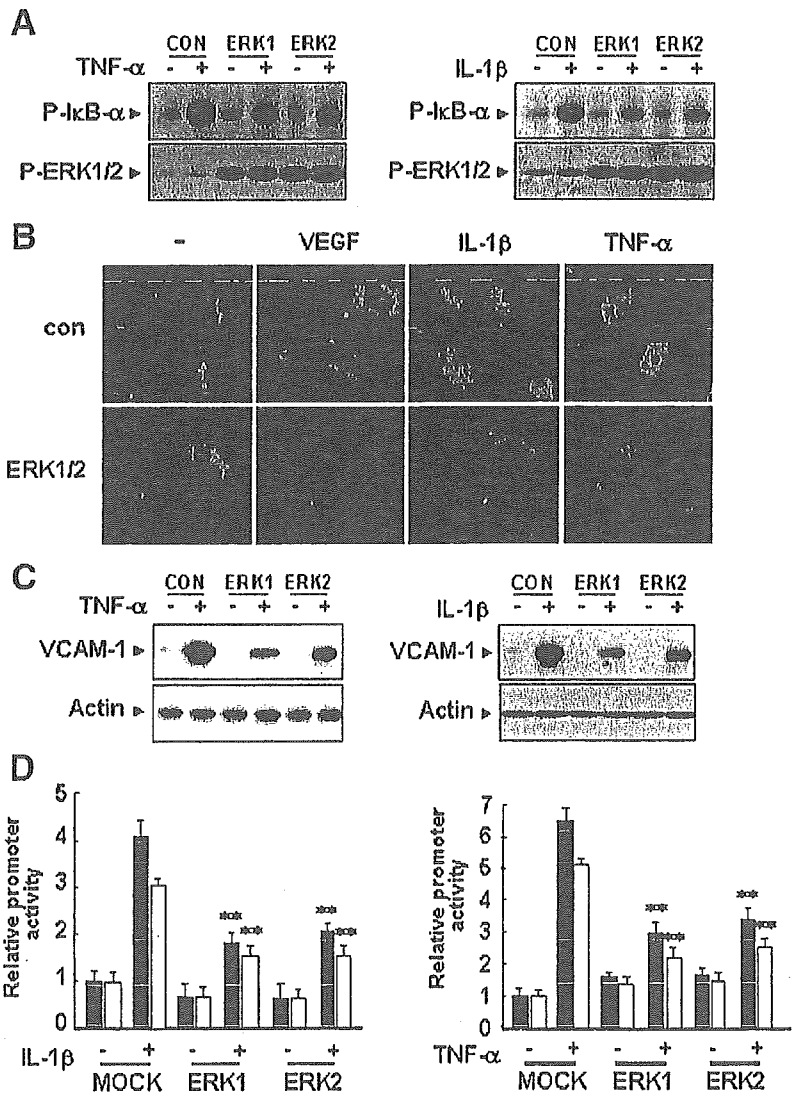

Fig. 5. Overexpression of ERK suppresses NF-κB activation and VCAM-1 expression in response to IL-1β and TNF-α. (A) HUVECs were transfected with ERK wild form (ERK1, 2) and then stimulated with 10 ng/ml TNF-α or 50 units/ml IL-1β for 10 min. Western blots were probed with anti-phospho-IκBα and anti-phospho-ERK antibodies. (B) Immunocytochemical analysis of p65 localization. HUVECs were transfected with ERKs wild form (ERK1, 2) and then stimulated with 10 ng/ml VEGF, 10 ng/ml TNF-α or 50 units/ml IL-1β for 30 min and subjected to immunocytochemistry as described in "Materials and methods". (C) HUVECs were transfected with ERKs wild form (ERK1, 2) and then stimulated with 10 ng/ml TNF-α or 50 units/ml IL-1β for 8 h. Western blots were probed with anti-VCAM-1 and reprobed with an anti-actin antibody to verify equal loading of protein in each. (D) HUVECs were cotransfected with pVCAM-1-Luc (fragment 6: 1.8 kilobase pair, fragment 3: 329 bp), a β-galactosidase plasmid, and a ERKs wild form (ERK1, 2). Twenty four hours after transfection, they were incubated with 10 ng/ml TNF-α or 50 units/ml IL-1β for 24 h. Luciferase activity was normalized to β-galactosidase activity. Data are means±S.D. of luciferase light units relative to control untreated cells (set at 100%) in quadruplicate experiments. **, $P<0.01$ versus MOCK+IL-1β or MOCK+TNF-α.

immunoprecipitates as described [28]. Cell stimulation with VEGF activated the ability of IKK to phosphorylate GST-IκBα (Fig. 3D). This VEGF-induced IKK activation was significantly increased by pretreatment of U0126 (Fig. 3D).

The dissociation of NF-κB from IκBα results in translocation of NF-κB to the nucleus, where it binds to specific sequences in the promoter regions of target genes. We next determined the effect of ERK inhibitors on VEGF-induced nuclear translocation and NF-κB DNA binding activity. VEGF caused nuclear translocation of the p65 subunit of NF-κB and this was significantly increased by pretreatment with PD98059 (Fig. 3E). Furthermore binding to target NF-κB oligonucleotides was also markedly augmented by pretreatment with PD98059 (Fig. 3F). PD98059 on its own had no effect on nuclear translocation and NF-κB DNA binding activity (Fig. 3E and F). Collectively, these results suggest that ERK suppresses VEGF-induced NF-κB activation by blocking the VEGF signaling pathway leading to IκBα phosphorylation.

3.4. PKC mediates both IκBα phosphorylation and ERK activation by VEGF

Our data indicate that VEGF induces both IκBα phosphorylation and ERK activation in endothelial cells. It was of interest to identify the upstream signaling molecules that lead to IKK and ERK activation. A previous study suggested the involvement of PKC in NF-κB activation leading to endothelial CAM expression [31,35,36]. We therefore examined the role of PKC in IκBα phosphorylation by employing two PKC inhibitors, GF109203X and chelerythrine chloride, and, in parallel, compared the effect of these inhibitors on VEGF-induced ERK activation. As shown in Fig. 4A, both IκBα phosphorylation and ERK activation in response to VEGF were inhibited by GF109203X and chelerythrine chloride, indicating that PKC lies upstream of both IKK and ERK. Under the same condition, U0126 completely inhibited ERK activation in response to VEGF, and increased the VEGF effect on IκBα phosphorylation (Fig. 4A). Similarly, VEGF-induced VCAM-1 expression was blocked by GF109203X and chelerythrine chloride, but increased by U0126 (Fig. 4B). These results suggest that in the VEGF signaling pathway PKC provides a positive signal activating IKK and ERK, a negative signal.

3.5. Overexpression of ERK suppresses NF-κB activation and VCAM-1 expression in response to IL-1β and TNF-α

The role of ERK pathway in other cytokine-induced NF-κB activation was explored. Unlikely to VEGF, IL-1β and TNF-α did not significantly induce ERK activation in HUVECs in contrast to their strong stimulatory activity on NF-κB. Consistently, inhibition of ERK by pretreatment of HUVECs with 5 μM U0126 did not further increase IκBα phosphorylation in response to either IL-1β or TNF-α (data not shown). However, overexpression of either wild type ERK1 or ERK2 markedly reduced both IL-1β-and TNF-α-induced IκBα phosphorylation (Fig. 5A). In addition, nuclear translocation of

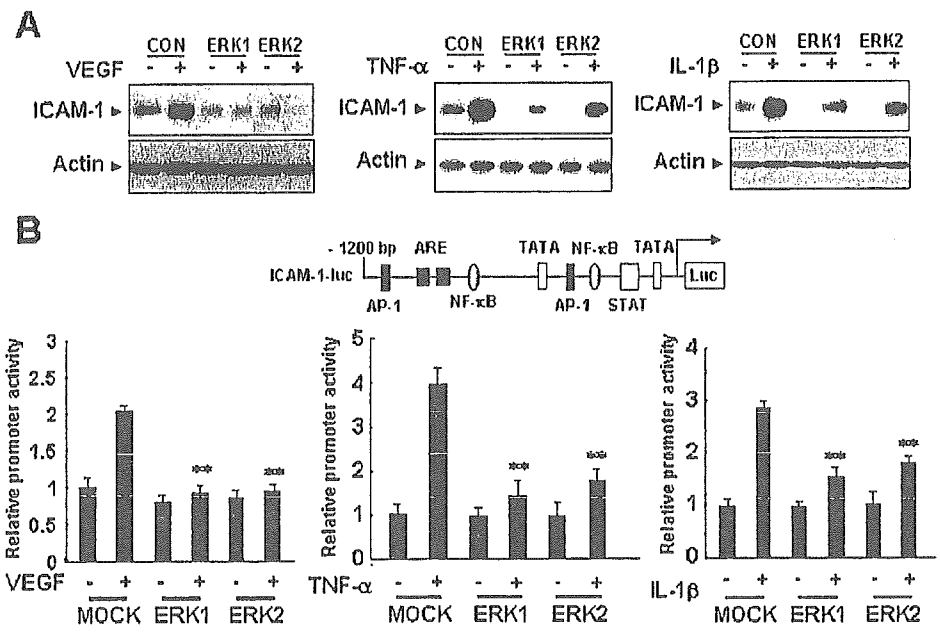

Fig. 6. ERK reduces endothelial ICAM-1 expression in response to VEGF, IL-1β, and TNF-α. (A) HUVECs were transfected with ERKs wild form (ERK1, 2) and then stimulated with 10 ng/ml VEGF, 10 ng/ml TNF-α or 50 units/ml IL-1β for 8 h. Western blots were probed with anti-ICAM-1 and reprobed with an anti-actin antibody to verify equal loading of protein in each. (B) HUVECs were cotransfected with pICAM-1-Luc (1.2 kilobase pair), a β-galactosidase plasmid, and a ERKs wild form (ERK1, 2). Twenty four hours after transfection, they were incubated with 10 ng/ml VEGF, 10 ng/ml TNF-α or 50 units/ml IL-1β for 24 h. Luciferase activity was normalized to β-galactosidase activity. Data are means±S.D. of luciferase light units relative to control untreated cells (set at 100%) in quadruplicate experiments. **, $P<0.01$ versus MOCK+VEGF, MOCK+IL-1β or MOCK+TNFα.

p65 subunit of NF-κB induced by either IL-1β or TNF-α was blocked by overexpression of ERKs (Fig. 5B). In agreement, both IL-1β and TNF-α increased endothelial VCAM-1 expression in a NF-κB dependent manner as shown in a promoter assay and these responses were significantly abrogated by overexpression of either ERK1 or ERK2 (Fig. 5C and D). These results raised the possibility that ERK negatively regulates NF-κB-dependent gene expression in endothelial cells through inhibiting the IκBα phosphorylation pathway stimulated by various agonists.

3.6. ERK reduces endothelial ICAM-1 expression in response to VEGF, IL-1β, and TNF-α

We further confirmed the role of ERK pathway on expression of other inflammatory genes in endothelial cells. ICAM-1 is one of representative endothelial cell adhesion molecules expressed in a NF-κB dependent mechanism. As expected, the protein level of ICAM-1 on HUVECs was increased by either treatment of VEGF, IL-1β or TNF-α (Fig. 6A). All these increases were almost completely or markedly

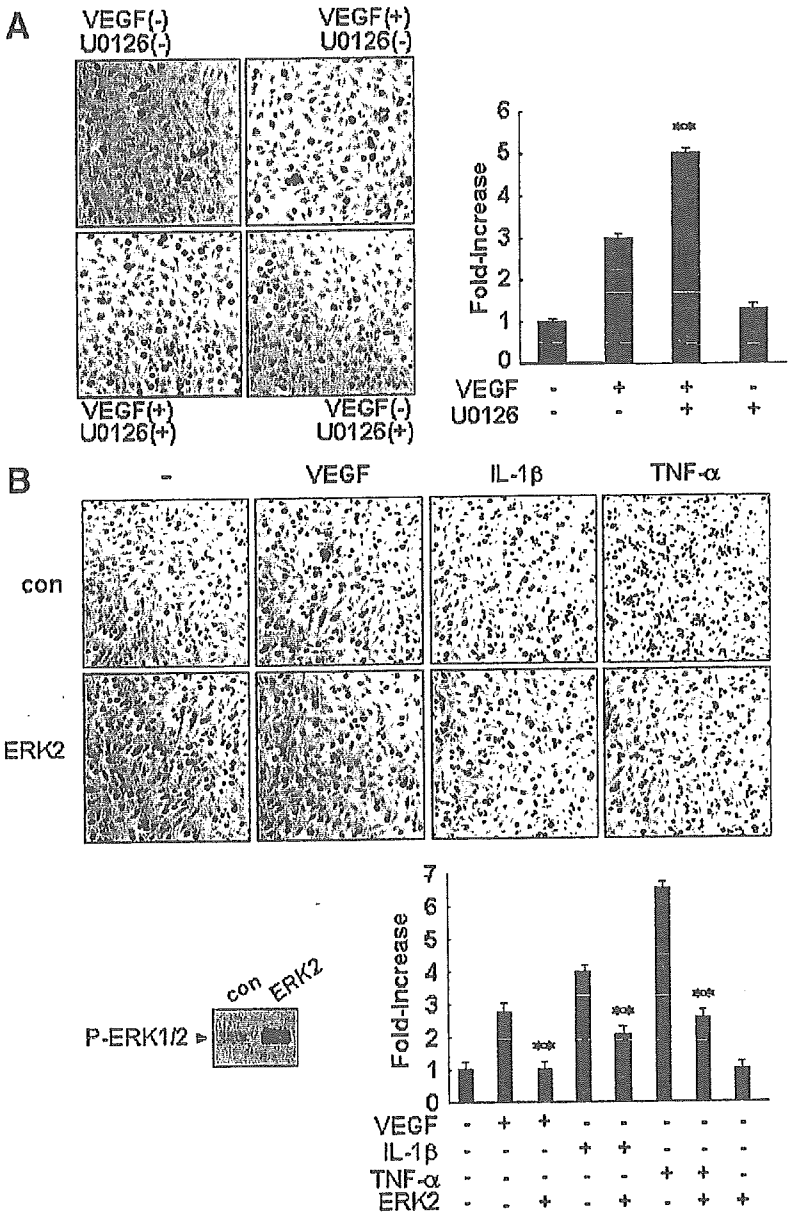

Fig. 7. ERK inhibitors increase VEGF-Induced leukocyte adhesion to endothelial cells. (A) HUVECs were preincubated for 30 min with or without 5 μM U0126 and then stimulated with 10 ng/ml VEGF for 8 h. (B) ERK2 lentiviral vectors were added to cell cultures at varying multiplicities of infection (MOIs ≈1–50). At 18 h, cells were washed and medium was replaced. HUVECs were stimulated with 10 ng/ml VEGF, 10 ng/ml TNF-α or 50 units/ml IL-1β for 8 h. Thereafter adhesion to U937 human monocytes was measured as described in "Materials and methods." Data are means±S.D. of adhesion relative to control untreated cells (set at 100%) in quadruplicate experiments. **, $P<0.01$ versus VEGF, IL-1β or TNF-α.

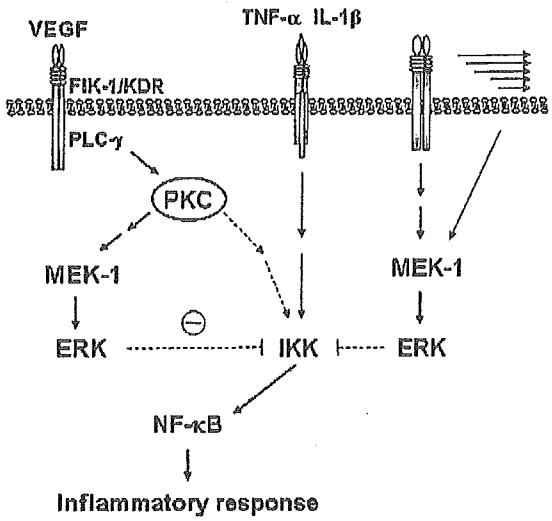

Fig. 8. Potential mechanism supporting anti-inflammatory role of ERK in the vascular wall.

inhibited by overexpression of either ERK1 or ERK2 (Fig. 6A). Consistently, ICAM-1-dependent transcriptional activities induced by these cytokines were inhibited by overexpression of ERK1 or ERK2 (Fig. 6B).

3.7. ERK inhibitors increase VEGF-Induced leukocyte adhesion to endothelial cells

Expression of CAMs, such as ICAM-1 and VCAM-1, on the surface of endothelial cells is required for endothelial–leukocyte interaction. Since inhibition of the ERK pathway increases the effect of VEGF on endothelial CAM expression, we tested whether the ERK inhibitor stimulates leukocyte adhesion to endothelial cells. HUVECs were exposed to 10 ng/ml VEGF for 8 h and then co-cultured with human monocytic U937 cells for an additional 1 h. As shown in Fig. 7, the adhesion of U937 cells to HUVECs was increased by VEGF, and this effect was accentuated by pretreatment with 5 μM U0126 (Fig. 7A). U0126 alone, on the other hand, had no effect (Fig. 7A). In contrast, overexpression of ERK2 markedly reduced VEGF-induced adhesion of U937 cells to HUVECs (Fig. 7B). Moreover, both IL-1β-and TNF-α-induced monocyte–endothelial cell interaction was also significantly reduced by overexpression of ERK2 (Fig. 7B). 4.

4. Discussion

Unveiling of endothelial NF-κB activation is pivotal for understanding the inflammatory reaction and the pathogenesis of inflammatory vascular diseases. A large number of studies have revealed the presence of a number of cellular stimuli, including inflammatory cytokines and oscillating shear stress, that lead to the endothelial NF-κB activation [10,37]. Conversely, factors such as angiopoietin-1, bFGF, hepatocyte growth factor (HGF), and normal lamina shear stress were shown to suppress NF-κB activation [38,39]. However, despite of a number of reports, precise understanding of their action mechanisms in the vasculature remains still unclear. Importantly, the present study demonstrates the novel role of ERK in controlling endothelial NF-κB activation and inflammatory gene expression.

Our data showed that inhibition of ERK increased VCAM-1 expression in response to VEGF stimulation, but that ERK inhibitors alone had no significant effect. This indicates that inhibition of ERK itself is incapable of stimulating VCAM-1 expression in endothelial cells, and suggests that VEGF sets in train both positive and negative signals related to VCAM-1 expression and that ERK may serve as an internal suppressor of the positive signal. Using two PKC inhibitors, it is clearly demonstrated that VEGF stimulates both ERK and IKK through PKC that lies downstream of KDR/Flk. Since ERK inhibits IKK activation by VEGF (Fig. 4), PKC seems to transmit both positive and negative signals involved in IKK activation. Therefore, the relatively weak activation of IKK and expression of inflammatory genes by VEGF is likely to be due to the concomitant activation of ERK. Similar phenomenon was observed in TNF-related activation-induced cytokine (TRANCE)-induced NF-κB activation and VCAM-1 expression. TRANCE stimulated ERK, IκBα phosphorylation, and transcriptional activity of NF-κB in HUVECs [40,41]. Pretreatment of the ERK inhibitors significantly enhanced TRANCE-induced NF-κB activation and VCAM-1 expression (data not shown), suggesting the suppressive role of concomitantly activated ERK in the cytokine-induced NF-κB pathway in endothelial cells.

Unlikely to VEGF, IL-1β and TNF-α had little effect on ERK activation in HUVECs, but they much strongly induced IKK activation and VCAM-1 expression compared to VEGF. The effects of IL-1β and TNF-α on IKK activation and VCAM-1 expression was very slightly increased by the ERK inhibitor (data not shown) but markedly suppressed by overexpression of ERK1 or ERK2. We also tested the effect of bFGF and EGF on VCAM-1 expression in HUVECs. These two growth factors markedly stimulated ERK activation in HUVECs, but did not induce VCAM-1 expression. In addition, ERK inhibitors had no significant effect on VCAM-1 expression (data not shown), presumably because these growth factors do not activate the NF-κB signaling pathway. We have recently reported that HGF counteracts VEGF-induced endothelial CAM expression through inhibiting IKK-mediated NF-κB activation [42]. HGF itself was unable to induce NF-κB activation but strongly stimulated ERK activation in endothelial cells (data not shown). In deed, it is observed that pretreatment of the ERK inhibitor prior to HGF administration results in reversing the inhibitory effect of HGF on VEGF-induced IκBα phosphorylation and VCAM-1 expression (data not shown). Although the precise mechanism engaged in agonists-dependent activation or inhibition of NF-κB pathway remains elusive, it is at least in part suggested that the cellular level of ERK activity may be one of crucial components to control IKK-mediated NF-κB activation in endothelial cells. Western blotting with antibodies against phospho-IκBα (Ser-32) and IκBα revealed that the ERK inhibitors increase IκBα phosphorylation at Ser-32 and degradation in response to VEGF (Fig. 4). Conversely, forced elevation of ERK activity in HUVECs resulted in the